REVIEW

Received 00th January 20xx,

Accepted 00th January 20xx

DOI: 10.1039/x0xx00000x

Glutathione peroxidase-like nanozymes: mechanism, classification, and bioapplication

Yifan Lai [a,†], Jingyu Wang[a,†], Ning Yue[a], Qiaochu Zhang[a], Jiangjiexing Wu[b,c,*], Wei Qi[a], and Rongxin Su[a,b,c,*]

The field of nanozymes is developing rapidly. In particular, glutathione peroxidase (GPx)-like nanozymes, which catalytically reduce H_2O_2/organic hydroperoxides to H_2O/alcohols, have attracted considerable attention. GPx-like nanozymes are powerful antioxidant enzymes known to combat oxidative stress. They have broad applications, including cytoprotection, anti-inflammation, neuroprotection, tumor therapy, and anti-aging. Although much progress has been made, GPx-like nanozymes have not been as well discussed or fully reviewed as other nanozymes. This review aims to summarize recent advances on GPx-like nanozymes from the vantage point of mechanism, classification, and bioapplication. Future prospects for advancing their design and application are also discussed.

1. Introduction

As critical secondary messengers in cell signal transduction, reactive oxygen species (ROS) are widespread *in vivo*.[1, 2] The most common ROS are superoxide anions ($O_2^{\bullet-}$), hydrogen peroxide (H_2O_2), hydroxyl radicals ($^{\bullet}OH$), and singlet oxygen ($^1O_2$).[3-5] To maintain normal physiological functions, ROS need to be at a suitable concentration.[6] When ROS build up in excess, oxidative cellular injury and cell death can occur, which is known as oxidative stress.[7, 8] Numerous studies have linked oxidative stress to a variety of diseases, including age-related,[9] neurodegenerative,[10, 11] inflammatory,[12] cardiovascular,[13] and diabetes.[14] The evolution of cells has left them with two antioxidant systems to scavenge ROS. One type of antioxidant is non-enzymatic, such as reduced glutathione (GSH), ascorbic acid, carotenes, *etc*.[15] The other type is antioxidant enzymes, mainly superoxide dismutase (SOD), catalase (CAT), and glutathione peroxidase (GPx).[16] One of the most interesting of them is GPx, which is known for its ability to scavenge H_2O_2.

GPx, an antioxidant enzyme, is responsible for maintaining the cellular redox balance. In 1957, GPx was identified as a protective factor for hemoglobin within erythrocytes.[17] Then, selenium was found to be essential to GPx.[18, 19] The identified crystal structure of GPx further revealed a catalytic active site containing selenium in the form of selenocysteine.[20] Studies on GPx showed that it could catalyze the reduction of H_2O_2/organic hydroperoxides to H_2O/alcohols under reduced GSH.[21] Consequently, it can be effective in inhibiting and fighting oxidative stress. It suffers, however, from various intrinsic defects as most natural enzymes, such as being too expensive, unstable, and difficult to mass produce.[22] Therefore, it is vital to explore GPx mimics extensively to overcome the limitations mentioned above and facilitate practical applications.[23]

Due to the discovery that GPx is a selenoenzyme, researchers initially looked at organoselenium compounds.[24-29] Other compounds, such as organotellurium compounds, have also been identified as potential GPx mimics.[30] Following the discovery in 2007 of magnetic Fe_3O_4 nanoparticles to possess peroxidase (POD)-like activity, nanozymes, nanomaterials with enzyme-like properties, have gained widespread attention.[31-35] Since nanozymes are low-cost, highly stable, multifunctional, and easy to mass produce, they are considered the next generation of artificial enzymes.[36-38] The discovery that V_2O_5 nanowires resemble GPx further catalyzed the breakthrough and opened up new possibilities.[39] As of today, GPx-like nanozymes have been explored and developed for applications including cytoprotection, anti-inflammation, neuroprotection, and tumor therapy (Scheme 1). In order to highlight the recent progress, an overview of the development of GPx-like nanozymes is provided. This review will cover GPx-like nanozymes' mechanism, classification, and bioapplications. A discussion on the challenges and future developing prospects of GPx-like nanozymes ends the paper.

[a] State Key Laboratory of Chemical Engineering, Tianjin Key Laboratory of Membrane Science and Desalination Technology, School of Chemical Engineering and Technology, Tianjin University, Tianjin 300072, P.R. China.
[b] Zhejiang Institute of Tianjin University, Ningbo, Zhejiang 315201, P.R. China.
[c] School of Marine Science and Technology, Tianjin University, Tianjin 300072, P.R. China.
Email: wujiangjiexing2007@126.com, wjjx1987@tju.edu.cn, surx@tju.edu.cn
†These authors contributed to this work equally.

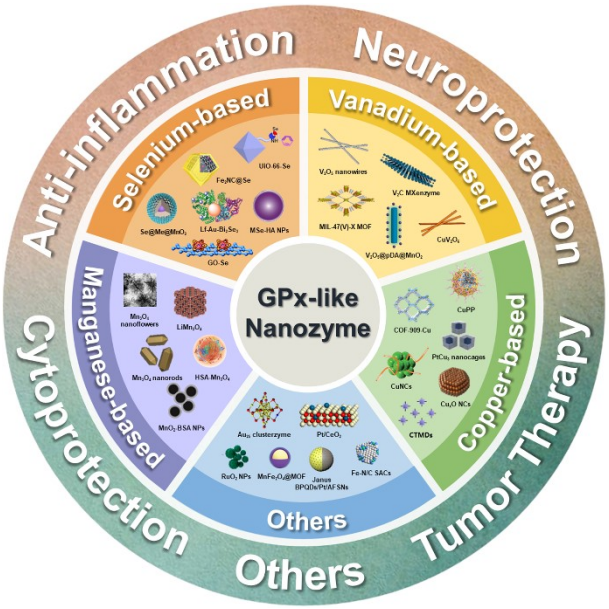

Scheme 1 Classification and bioapplications of GPx-like nanozymes.

2. Mechanisms of GPx-like nanozymes

Over the past few decades, natural GPx catalytic mechanisms have been investigated extensively. There is a ping-pong mechanism[40] as well as an ordered mechanism[41] in natural GPx's catalysis of multi-substrate reactions. However, while many nanomaterials mimicking GPx have been developed, their catalytic mechanisms have not received as much attention. Studies conducted so far suggest that GPx-like nanozymes have two catalytic mechanisms. The ping-pong and ordered mechanisms will be discussed in this section.

2.1 Ping-pong mechanism

It was reported in the early 1970s that Flohé and co-workers found that GPx1 in bovine red blood cells used a ping-pong mechanism.[40] In this mechanism, substrates and products alternately bind to or release from the enzyme. Further studies showed that the catalytic schemes of GPx1, GPx3, and GPx4 can all be represented by a catalytic cycle, as shown in Fig. 1A.[42] Hydroperoxides oxidized the active center of -SeH to -SeOH, which was then reduced by a molecule of GSH to -SeSG. This then reset the catalytic process to start over with another GSH molecule. In the same way as natural GPx, several studies have shown that some GPx-like nanozymes use the ping-pong mechanism, where hydroperoxide oxidizes their active sites to form peroxide intermediates.[39, 43-50] As an example, see Fig. 1B for the catalytic cycle of V_2O_5 nanowires.[39] The first step was to react with H_2O_2 on the active surface to produce vanadium peroxide intermediate 1, followed by a GSH attack to produce sulfonate-bound intermediate 2. In contrast to natural GPx, intermediate 2 was hydrolyzed into glutathione sulfenic acid (3, GSOH) and a dihydroxo intermediate 4, which underwent a redox reaction with another H_2O_2 to yield intermediate 1. At the same time, GSOH would react with another GSH molecule to form glutathione disulfide (GSSG). In the catalytic process, the interaction between H_2O_2 and active site V=O to form vanadium peroxide is of great importance.

In some cases, however, peroxide intermediates would not form at all. This is because the active site would first interact with GSH rather than H_2O_2, changing its redox state. Typical examples are the GPx-like catalytic reactions of CuV_2O_6 with GSH and H_2O_2, which differ greatly from the previously reported V_2O_5 nanowires.[51] As shown in Fig. 2A and B, the absence of peaks at 1150 cm^{-1} and 930-940 cm^{-1} in Raman and infrared spectra indicated that no V-peroxide species formed. Additional X-ray photoelectron spectroscopic analysis of CuV_2O_6 interacting with GSH and extra H_2O_2 allowed further investigation of the intermediates (Fig. 2C and D). Following interaction with GSH, the valence state of V was clearly exhibited as +IV, and after the addition of excess H_2O_2, both +V and +IV products were formed. Fig. 2E shows the two equations corresponding to the reactions involved. According to the above results, the GPx-like activity

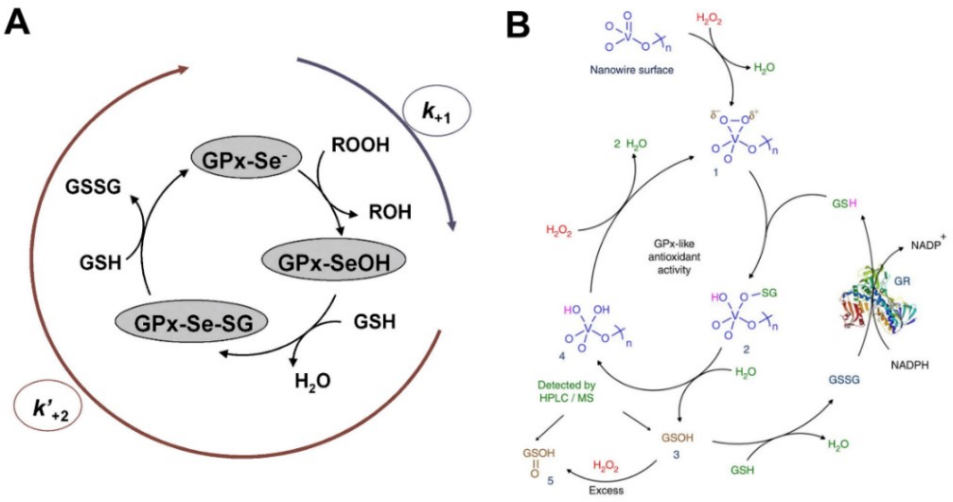

Fig. 1 (A) Ping-pong mechanism of natural GPx. Reprinted with permission from ref. 42. Copyright (2013) Elsevier. (B) A catalytic mechanism for V_2O_5 nanowires to exhibit GPx-like activity. Reprinted with permission from ref. 39. Copyright (2014) Springer Nature.

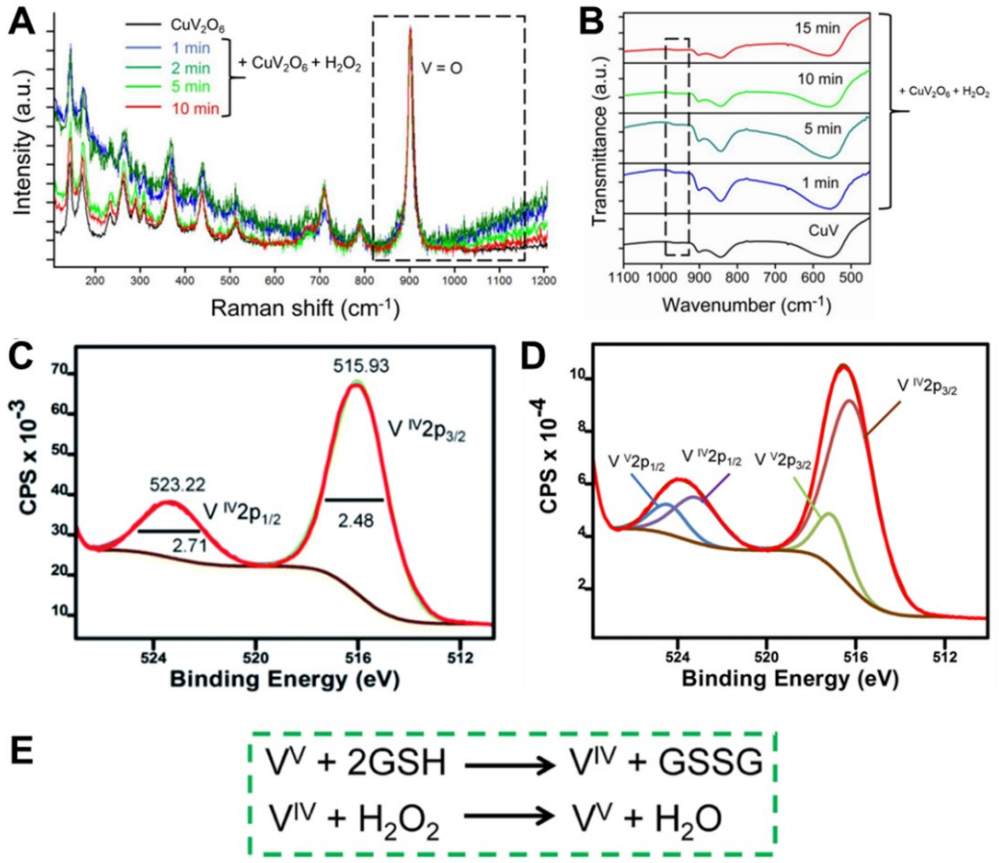

Fig. 2 (A and B) Changes in the Raman and infrared spectra of CuV_2O_6 reacting with H_2O_2 with time. (C and D) X-ray photoelectron spectroscopic analysis of V2p after CuV_2O_6 has been treated with 10 mM GSH and 0.1 M H_2O_2, respectively. (E) Catalytic equations for the GPx-like activity of CuV_2O_6. Adapted with permission from ref.51. Copyright (2022) Royal Society of Chemistry.

of CuV_2O_6 was caused by a redox change in the vanadium center. The redox valence changes of active centers have also been observed in other types of nanozymes, such as Mn-,[52] Cu-,[53, 54] Ru-based,[55] *etc.* In some bimetallic nanozymes, both active sites would produce valence redox changes.[56-58] As an example, Sn^{2+}/Sn^{4+} and Fe^{2+}/Fe^{3+} redox couples played an important role in catalyzing the GPx-like reaction of $SnFe_2O_4$.[57]

2.2 Ordered mechanism

Santimone and co-workers argued in 1997 that GPx worked as a sequential ordered mechanism, rather than a ping-pong one.[41] A sequenced mechanism involves binding multiple substrates to the enzyme in a specific order to form an enzyme-multisubstrate multiplex intermediate, and the product is only released after all substrates are bound to the enzyme. In specific, GPx would combine with one molecule of H_2O_2 and two molecules of GSH, resulting in GSSG and E during one catalytic cycle (Fig. 3A). Of all the studies conducted on GPx-like nanozymes, one involved GPx-like nanozymes that followed an ordered mechanism.[59] By modifying Au NPs with selenium-containing pentapeptides, GPx-like nanozymes were constructed (Fig. 3B). The kinetics study with parallel lines in Fig. 3C and D indicated the mechanism of ping-pong for such selenopeptides. As pentapeptides immobilized on Au NPs to form GPx-like nanozymes, kinetics analysis of the crossed lines in Fig. 3E and F revealed an ordered mechanism. The altered mechanism may be the result of Au NPs scaffolds constraining the peptide mobility and conformation, exposing more active sites to co-interact with the substrates.

3. Types of GPx-like nanozyme

As a result of studying natural GPx and developing nanozymes, multiple nanomaterials that possess GPx-like properties have been developed (Fig. 4). The small organoselenium and organotellurium compounds have already been reviewed in detail,[60-62] and are not discussed in this review. To simplify the classification of GPx-like nanozymes, the active center element is used as the basis for five categories: (1) selenium-based, (12) vanadium-based, (3) manganese-based, (4) copper-based, and (5) others. Detailed categories can be found in Table 1 and their available kinetics parameters are shown in Table 2.

3.1 Selenium-based

Since selenium was proven essential for natural GPx, organoselenium compounds have often been used as GPx mimics.[63] These compounds were further installed onto various nanoscale scaffolds, including micelles, vesicles, polymer nanoparticles, and superamphiphile-assembled nanotubes, to improve

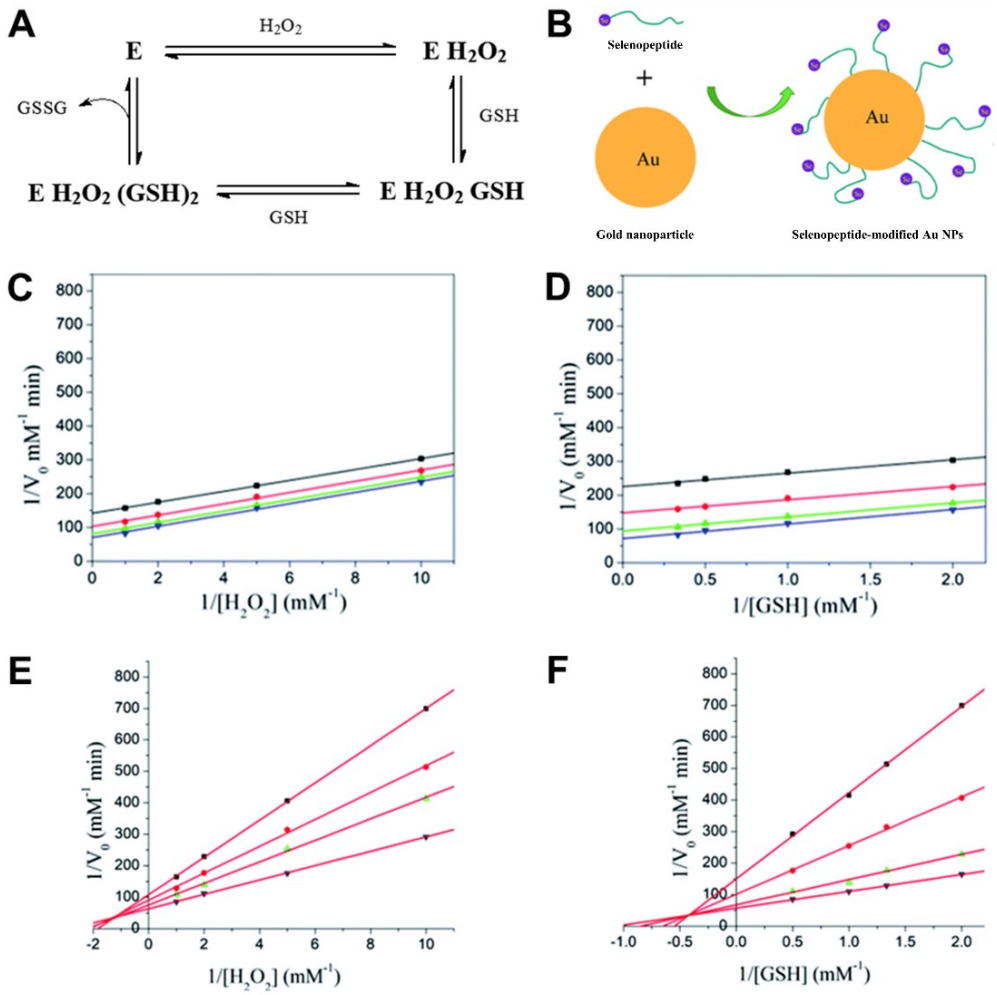

Fig. 3 (A) The flow chart of the ordered mechanism. Adapted with permission from ref. 41. Copyright (2004) John Wiley and Sons.-(B) The construction of selenopeptide-modified Au NPs. (C and D) The double-reciprocal plots of GPx-like activity for selenopeptides. (E and F) The double-reciprocal plots of GPx-like activity for selenopeptide-modified Au NPs. Adapted with permission from ref. 59. Copyright (2020) Royal Society of Chemistry.

catalytic efficiency. Having highly ordered and moderately flexible structures, these scaffolds provided binding sites and a proper microenvironment, and thus enhanced the catalytic activity.[64-69] Adding stimuli-responsive polymers to the scaffold could allow its catalytic efficiency to be reversibly controlled by external conditions, such as temperature, pH, light, or ionic strength.[70] More recently, the development of nanotechnology has led to the use of nanomaterials as nano-scaffolds, including graphene oxide (GO),[71] the metal–organic framework (MOF) UiO-66,[72] and gold nanoparticles (Au NPs).[59] As shown in Fig. 5A, phenylselenylbromide was covalently linked to organic ligands of UiO-66-NH_2 to obtain selenium-functionalized UiO-66-Se. The high specific surface area and uniform porosity of UiO-66-Se allowed it to offer more catalytic active centers and exhibit better GPx-like activity.[72] An interesting aspect of such a Se-containing molecule is that it can also bind with metal to form MOF structures and exhibit GPx-like properties. As seen in Fig. 5B, Se-containing diimidazole ligands assembled with Zn^{2+} to form Se-MOF as the Fe_2NC shell. This shell would not only provide the GPx-like activity, but also enhance the stability and biocompatibility of Fe_2NC.[73]

Also, selenium nanoparticles (Se NPs) and metal selenides (*e.g.*, Bi_2Se_3, $MoSe_2$, and Mo_3Se_4) were used to mimic GPx.[43, 74-77] By adding ascorbic acid to a GO/selenium dioxide solution, Qu, Ren, and co-workers fabricated GO-Se nanocomposites in which Se NPs were well modified on the surface of GO. As demonstrated by the typical glutathione reductase (GR) coupled assay, Se NPs had GPx-like activity, and GO's large surface area and rapidly transferring electrons could enhance the activity (Fig. 5C and D).[43] As well as GO, some surface coatings and modifications were also used to improve the dispersion and stability, such as polyvinylpyrrolidone (PVP),[75, 76] polydopamine (pDA),[44, 78] hyaluronic acid (HA),[45] and polysaccharides.[79] The coating or modification would even serve as a synergistic antioxidant. The synergetic antioxidant machinery in organisms, for instance, inspired Qu, Ren, and co-workers to develop pDA coated Se NPs, which acted as non-enzymatic antioxidants and antioxidant enzymes, respectively. By exploiting the $O_2^{\bullet-}$ and $^{\bullet}OH$ scavenging properties of pDA, Se@pDA nanocomposites demonstrated more potent antioxidant capacity. An application of this synergistic antioxidant system will be described in the Application section.[44]

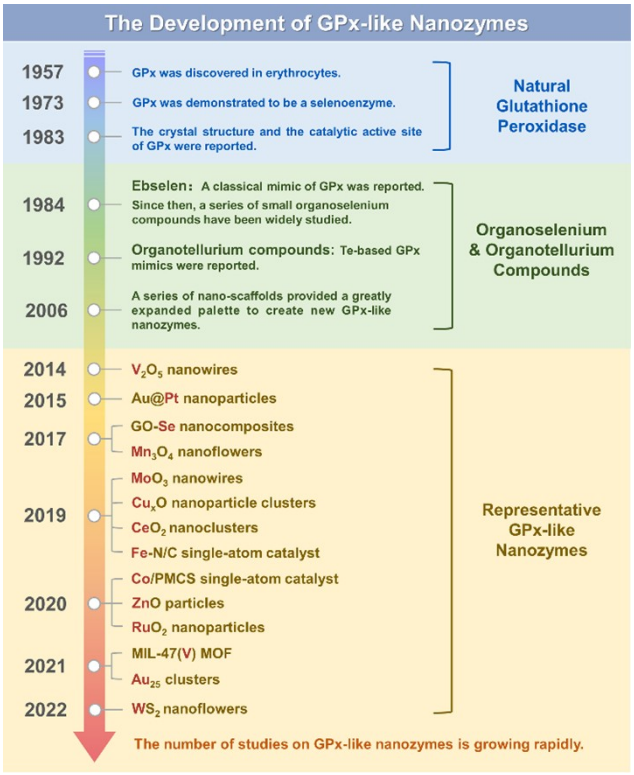

Fig. 4 A brief timeline for the development of GPx-like nanozymes (natural and artificial enzymes are listed for better understanding). Note: for each active atom, only representative nanomaterials are listed, and more detailed information can be found in Table 1.

3.2 Vanadium-based

Mugesh, D'Silva, and co-workers first reported in 2014 that V_2O_5 nanowires could exhibit GPx-like activity and exert cytoprotective effects effectively.[39] Subsequent studies indicated that different morphologies and crystal planes would influence this activity.[46] As shown in Fig. 6A, nanowires (VN_w), nanoflowers (VN_f), nanosheets (VS_h), and nanospheres (VS_p) were synthesized with different exposed crystal facets. The VN_w only had {001} facets, the VN_f had major {010} and minor {001} facets, the VS_h had major {001} and minor {010} facets, and the VS_p had two major {010} and {100} facets. The GPx-activities of these four V_2O_5 nanozymes followed the order: VS_p > VN_f > VS_h > VN_w, seeing Fig. 6B. A detailed study based on experiments and theoretical calculations found that {010} and {100} facets were more active than {001} because of their unsaturated surfaces, with {010} being the most active.

Following these pioneering studies, other V-based nanomaterials, such as V_2C MXenzyme,[47, 80] orthovanadate NP,[81, 82] MIL-47(V) MOF,[48] VN_4 single-atom,[83] MnV_2O_6,[51] ZnV_2O_6,[51] and CuV_2O_6,[51] also exhibited excellent GPx-like activities. As shown in Fig. 6C, a MIL-47(V)-H MOF nanozyme mimicking GPx was synthesized by coordinating the 1,4-benzenedicarboxylicacid ligand with V^{3+} and modulated its GPx-like activity by ligand engineering.[48] In particular, F, Br, NH_2, CH_3, and OH were substituted for H in the benzenedicarboxylicacid ligand to create MIL-47(V)-X MOFs (X = F, Br, NH_2, CH_3, OH, and H). Their GPx-like activities were then investigated and shown in Fig. 6D. These isostructural MOFs all exhibited GPx-like activity, and the substitutions enhanced the catalytic activity, with MIL-47(V)-NH_2 being the most active. In addition, a control experiment using only ligands was conducted under identical conditions to clarify why MIL-47(V)-X MOFs differ in their catalytic activity. It is unlikely that ligands alone would have GPx-like activities, ruling out the possibility that their intrinsic catalytic activity could influence the results. As a result of the X-ray photoelectron spectroscopy results and subsequent analysis, the electronic impact of substitution on the metal nodes was found to be responsible for the difference in catalytic activity between the MIL-47(V)-X MOFs.

3.3 Manganese-based

GPx's activity was first reported to be efficiently mimicked by Mn_3O_4 nanoflowers by Mugesh, D'Silva, and co-workers in 2017.[84] GPx mimicking manganese oxides has been widely reported since then, mainly using Mn_3O_4.[49, 52, 84-87] In comparison to Mn_3O_4, other manganese oxides, such as MnO,[52] MnO_2,[52, 88] Mn_2O_3,[52] and $ZnMn_2O_4$,[89] have been investigated less due to their lower activities. It is believed that GPx-like activity was related to the mixed valence states and redox cycling of Mn(II) and Mn(III).[52] Through valence engineering, Wei and co-workers modulated $ZnMn_2O_4$ to show GPx-like activity (Fig. 7A).[89] A series of Li-doped samples were obtained through hydrothermal synthesis, and these $Zn_{1-x}Li_xMn_2O_4$ (x = 0, 0.2, 0.4, 0.6, and 1) were denoted by ZM, Li-2, Li-4, Li-6, and LM. According to the catalytic activity test results, more Li doping resulted in higher GPx-like activity, while LM exhibiting the highest activity. In contrast, ZM, the initial material, and Li-2, the low-doped sample, did not exhibit GPx-like properties (Fig. 7B). A more detailed valence analysis revealed a correlation between the increase of the activity and the change in Mn's valence. The addition of Li changed the valence state of Mn from Mn^{3+} to Mn^{4+}, which was associated with higher GPx-like activity.

Besides valences, other factors may play an important role in modulating the GPx-like activities of manganese oxide nanozymes. For example, Mn_3O_4 with different morphologies, including cubes, polyhedra, hexagonal plates, flakes, and flowers, exhibited different GPx-like activities, following the order: flowers > flakes > hexagonal plates ≈ polyhedra ≈ cubes (Fig. 7C).[52] The higher activity of flowers and flakes was due to the more active sites and higher electrical conductivity than the other three morphologies. Another study conducted by Sun and co-workers demonstrated that the GPx-like activity of Mn_3O_4 nanoparticles was related to the crystal facet.[87] They synthesized three morphologies, including nanospheres, nanocubes, and nanorods, that were encircled by {101}, {200}, and {103} crystal facets. The results demonstrated that GPx-like activity of {103}-faceted nanorods was superior to that of {101}-faceted nanospheres and {200}-faceted nanocubes. This is attributed to the increased reaction energy of the Mn_3O_4 nanorods surface, which had superior ROS scavenging capability.

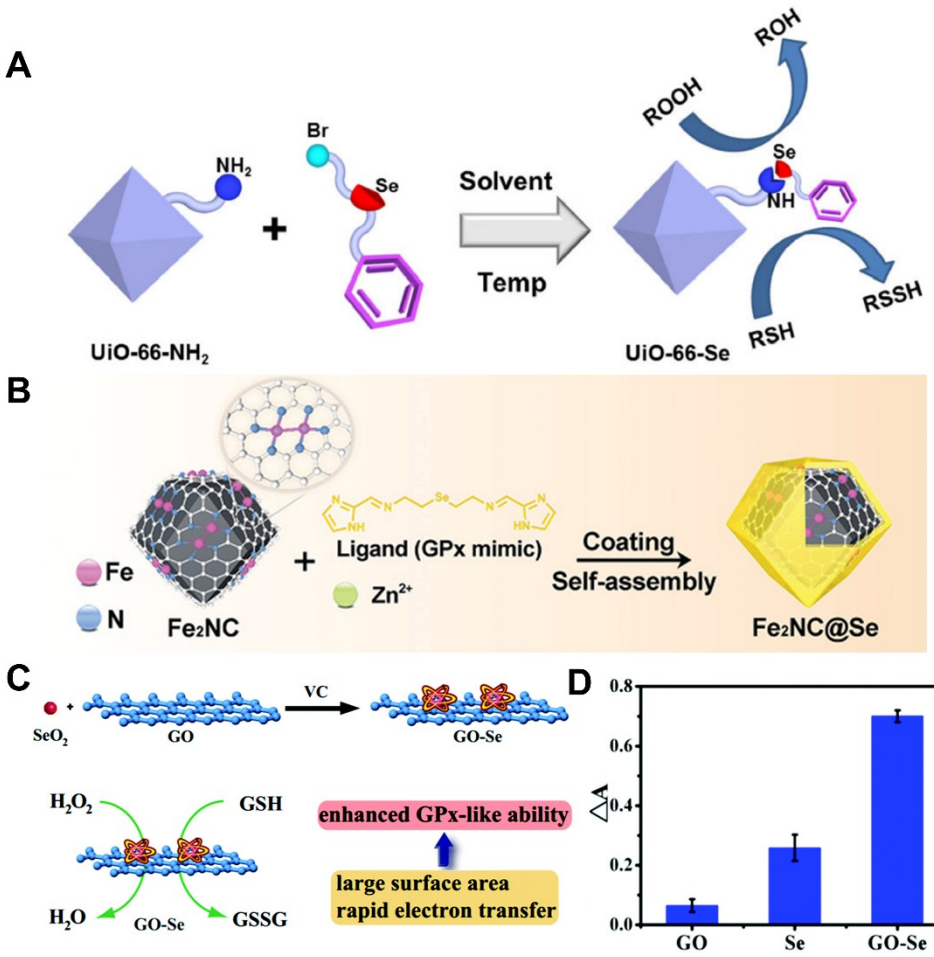

Fig. 5 (A) An illustration of how UiO-66-Se is synthesized. Reprinted with permission from ref. 72. Copyright (2018) Springer Nature. (B) Schematic illustration of the synthesis of Fe2NC@Se. Adapted with permission from ref. 73. Copyright (2022) John Wiley and Sons. (C and D) Diagram illustrating GO-Se nanocomposite synthesis and GPx-like activity. Adapted with permission from ref. 43. Copyright (2017) Royal Society of Chemistry.

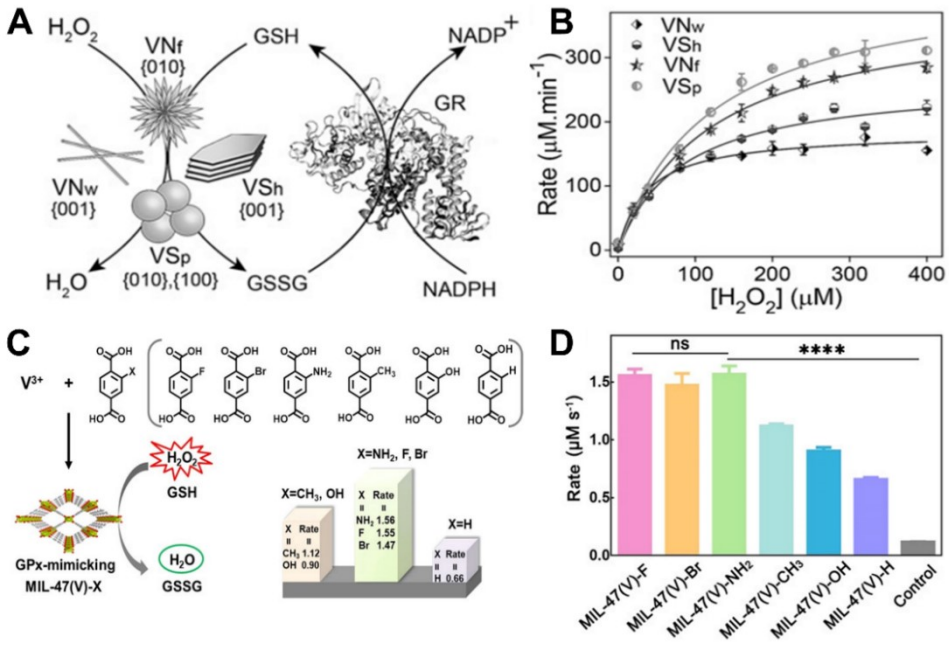

Fig. 6 (A and B) GPx-like activities of different V_2O_5. Adapted with permission from ref. 46. Copyright (2018) John Wiley and Sons. (C and D) A schematic of the synthesis of MIL-47(V)-X MOFs and their GPx-like activities. Adapted with permission from ref. 48. Copyright (2021) John Wiley and Sons.

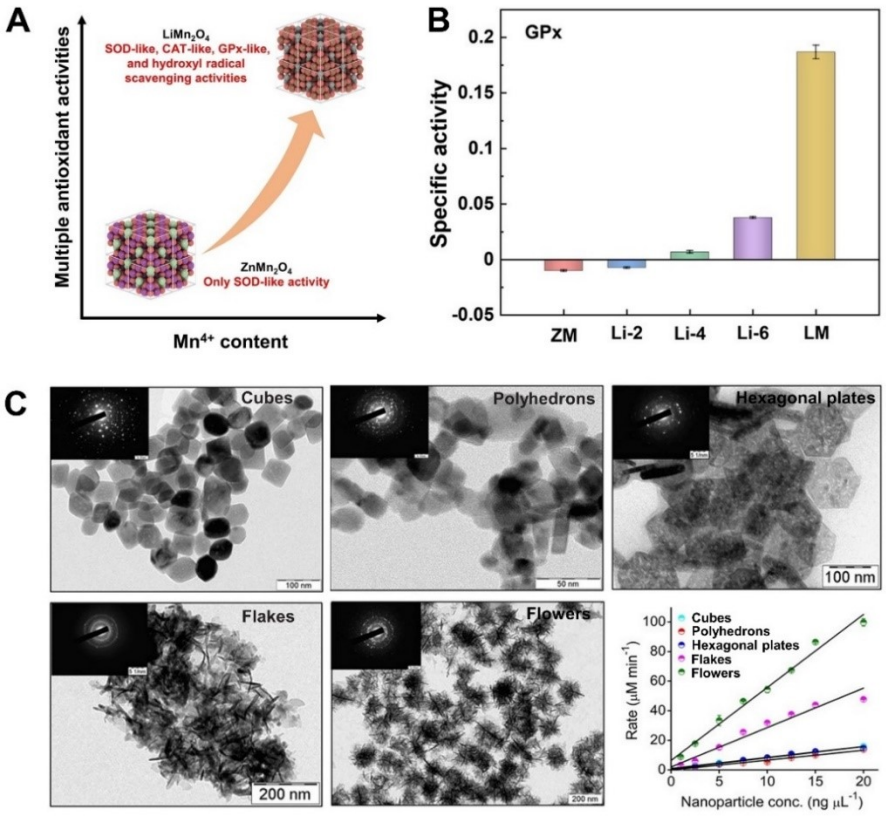

Fig. 7 (A and B) An illustration of the valence-engineering strategy for modulating the GPx-like activity of Li-doped samples. Adapted with permission from ref. 89. Copyright (2022) John Wiley and Sons. (C) TEM images of Mn_3O_4 with different morphologies and their GPx-like activities. Adapted with permission from ref. 52. Copyright (2018) John Wiley and Sons.

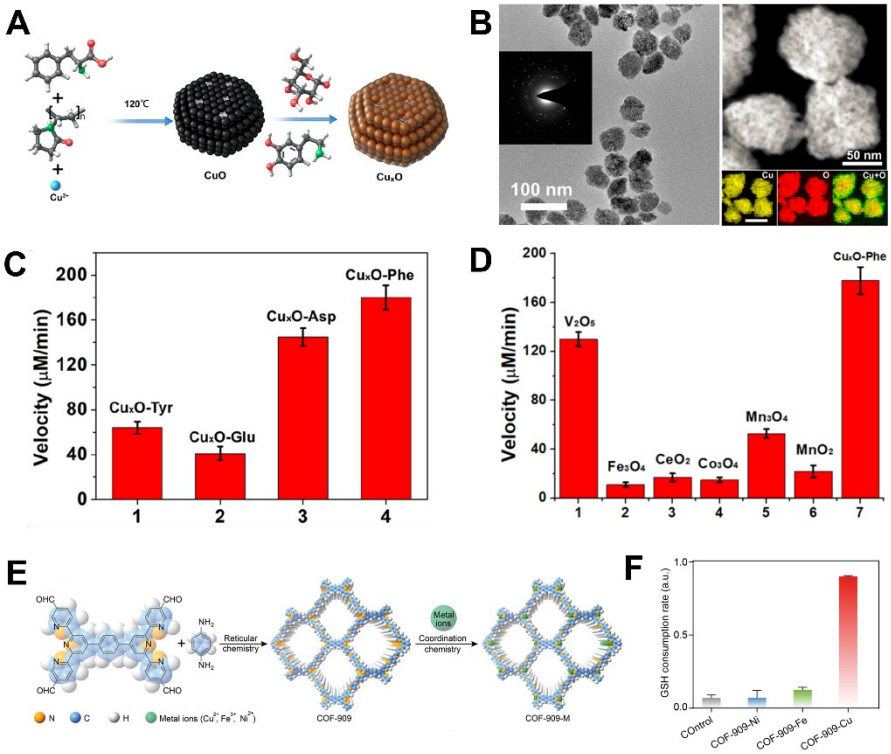

Fig. 8 (A and B) An illustration of the synthesis of Cu_xO-Phe and its morphology. (C and D) GPx-like activities of various Cu_xOs and other metal oxides. Adapted with permission from ref. 90. Copyright (2019) American Chemical Society. (E and F) Schematic illustration of different metal-containing COFs and their GPx-like activities. Adapted with permission from ref. 98. Copyright (2022) John Wiley and Sons.

3.4 Copper-based

As with manganese oxides, copper oxides also exhibited GPx-like properties.[51, 90-94] As an example, a Cu_xO nanozyme as GPx mimics was synthesized with phenylalanine (Phe).[90] The reaction of Cu(II) ions, Phe, and PVP took place at 120 °C, and then partial reduction with glucose was conducted to create Cu_xO (Fig. 8A). The formed Cu_xO nanozyme had a porous structure with an average diameter of 65 nm (Fig. 8B). If the structure-directing agent was changed from Phe to another amino acid or none at all, the final structure would appear in different morphologies and sizes. In particular, tyrosine (Tyr) and aspartic acid (Asp) would form ellipsoids with a mean size of 100 nm, glutamic acid (Glu) would form rods, no ligand would form sheets, while lysine and arginine could not form uniform nanoparticles. A comparison of the GPx-like activity of these different Cu_xOs indicated that Cu_xO-Phe was the most active, and also superior to Mn_3O_4 and V_2O_5 (Fig. 8C and D). Further analysis revealed that the higher surface area, unique porous structure, and even Phe ligand contributed to the highest activity. In this study, Cu_xO was a complex of CuO and Cu_2O. Similarly, $Cu_{5.4}O$, synthesized by reducing Cu^{2+} using L-ascorbic acid to form a complex of Cu and Cu_2O, acted as a GPx mimic as well.[92, 93]

Furthermore, other Cu-containing nanomaterials, such as MOF nanodots,[95] $PtCu_3$ nanocages,[53] Cu nanoclusters,[96] Cu-doped polypyrroles,[54] and covalent organic frameworks (COFs),[97, 98] exhibited excellent GPx-like properties. In a variety of fields, COFs have attracted widespread attention for their inherent porosity, high crystallinity, wide functionality, and strong biocompatibility. It is also possible to make GPx mimics by replacing N-doped carbon with COF, i.e., by decorating Cu^{2+} into COF scaffolds. As shown in Fig. 8E, COF-909-Cu was recently synthesized by Sun, Deng, and co-workers through decorating Cu^{2+} into COF-909 via a post-modification method.[98] In comparison to COF-909, COF-909-Ni, and COF-909-Fe, COF-909-Cu exhibited the highest GPx-like activity (Fig. 8F).

3.5 Others

Besides the nanomaterials mentioned above, many other nanomaterials also display GPx-like activity. Similar to selenium, tellurium-containing GPx-like nanozymes have also been constructed by combining tellurium-containing catalytic centers with nano-scaffolds.[99-102] Recent reports are revealing different active atoms in GPx-like nanozymes, including Au, Ce, Co, Fe, Mo, Pt, Ru, *etc.*[50, 55, 103-115] For example, the widely studied SOD- and CAT-like CeO_2 is seldom reported for its GPx-like activity. A study undertaken in 2019 by Ming, Zhang, and co-workers showed that CeO_2 exhibited GPx-like activity and that single-atom Pt doping further increased the initial reaction rate from 15.89 to 22.07 μM·min^{-1} (Fig. 9A and B).[105] The GPx-like activity of CeO_2 was subsequently investigated with various doping metal elements, and it was found that the highest performance was achieved after 10% Cr-doping (Fig. 9C and D).[106] This modification inspired the development of bimetallic nanoclusters[103, 104] or bimetallic oxides,[56-58, 116, 117] with modulated GPx-like properties. More interestingly, some GPx-like nanozymes, composed of two or more active elements, were investigated to show synergistic effect on their activity due to the increase of the number of redox couples. For example, $MnFe_2O_4$ with two redox couples (Mn^{2+}/Mn^{4+} and Fe^{2+}/Fe^{3+}) exhibited improved GPx-like activity because both Fe^{3+} and Mn^{4+} were able to react with GSH to form Fe^{2+}, Mn^{2+}, and GSSG.[56] Besides, two-dimensional transition metal dichalcogenides such as MoS_2 nanosheets and WS_2 nanoflowers were also shown to be GPx-like.[112, 118]

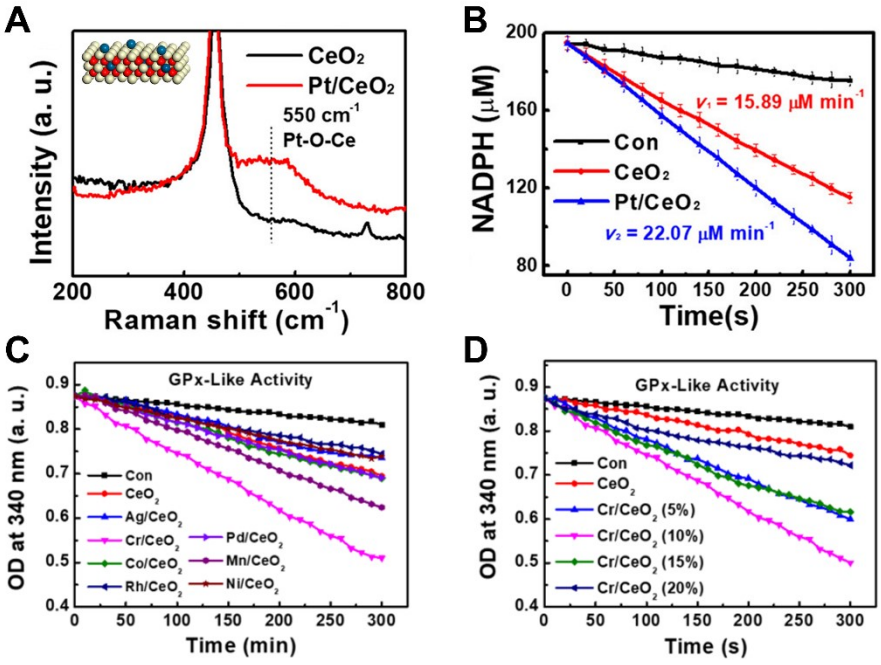

Fig. 9 (A and B) Successful synthesis of CeO_2 and Pt/CeO_2, as well as their GPx-like activities. Adapted with permission from ref. 105. Copyright (2019) American Chemical Society. (C) GPx-like activities of CeO_2 and different metal-doped CeO_2. (D) GPx-like activities of Cr/CeO_2 nanozymes with varying doping concentrations. Adapted with permission from ref. 106. Copyright (2021) Ivyspring International Publisher.

Table 1 Summary of GPx-like nanozymes

Active atom	Nanozyme	Types of enzyme-like activities	Application	Function of GPx-like activity	Ref.
Au	$Au_{24}Ag_1$ clusterzyme	GPx/CAT	Relieving acute neuroinflammation and treating trauma brain injury	Scavenging H_2O_2 and lipid peroxides	104
	Au_{25} clusterzyme	GPx (highest)/CAT/SOD	Relieving acute neuroinflammation and treating trauma brain injury	Scavenging H_2O_2 and lipid peroxides	103, 104
	$Au_{24}Cd_1$ clusterzyme	GPx/CAT/SOD (highest)	Relieving neuroinflammation by inhibiting interleukin (IL)-1β and IL-6	Scavenging H_2O_2 and lipid peroxides	103
	$Au_{24}Cu_1$ clusterzyme	GPx/CAT (highest)/SOD	Relieving neuroinflammation by inhibiting tumor necrosis factor (TNF)-α	Scavenging H_2O_2 and lipid peroxides	103
Ce	CeO_2	GPx/CAT/POD/SOD	Relieving neuroinflammation and treating trauma brain injury noninvasively	Scavenging H_2O_2 and synergizing with SOD- and CAT-like activities to eliminate oxidative stress	105, 106
	Cr/CeO_2	GPx/CAT/POD/SOD	Relieving neuroinflammation and treating trauma brain injury noninvasively	Scavenging H_2O_2 and synergizing with SOD- and CAT-like activities to eliminate oxidative stress	106
	Pt/CeO_2	GPx/CAT/POD/SOD	Relieving neuroinflammation and treating trauma brain injury noninvasively	Scavenging H_2O_2 and synergizing with SOD- and CAT-like activities to eliminate oxidative stress	105
	PEG/Ce-Bi@DMSN	GPx/CAT/POD	Relieving tumor hypoxia and depleting overexpressed GSH for tumor therapy	Depleting overexpressed GSH to decrease the scavenging of ROS and improve $^{\bullet}OH$-mediated tumor nanocatalytic therapy	119
Co	Co/PMCS	GPx/CAT/SOD	Alleviating systematic inflammation and treating sepsis	Scavenging H_2O_2 and synergizing with SOD- and CAT-like activities to eliminate oxidative stress	107
	COF-618-Cu	GPx/CAT	Relieving tumor hypoxia and depleting overexpressed GSH for tumor therapy	Depleting overexpressed GSH to decrease the scavenging of ROS and improve photodynamic and photothermal therapy efficacy	97
	COF-909-Cu	GPx/POD/SOD	Elevating H_2O_2 levels and inducing pyroptosis for tumor therapy	Depleting overexpressed GSH	98
	Cu nanoclusters (Cu NCs)	GPx/CAT/POD/SOD	Defending cells from oxidative stress by scavenging excess ROS	Scavenging H_2O_2 and fine-tuning the concentration of H_2O_2 for cell signalling	96
	Cu-TCPP MOF nanodots (CTMDs)	GPx/SOD	Alleviating acute kidney injury during endotoxemia	Scavenging H_2O_2 at the inflammatory sites and avoiding the toxicity of SOD-like activity	95
	Cu-doped polypyrrole (CuPP)	GPx/CAT/POD	Relieving tumor hypoxia and reprogramming macrophage for tumor therapy	Depleting overexpressed GSH to decrease the scavenging of ROS and improve $^{\bullet}OH$-mediated tumor immunotherapy	54
Cu	CuO NP-polyoxometalate (POM)	GPx/CAT/OXD/POD	Constructing multi-function sensors and sensing ascorbic acid and Fe^{2+}	Constructing a fluorometric sensor for Fe^{2+}	94
	CuO, Cu_2O	GPx	-	-	51
	Cu-O nanoparticle clusters	GPx/CAT/POD/SOD	Inhibiting neurotoxicity and ameliorating Parkinson's	Scavenging H_2O_2 and synergizing with SOD- and CAT-	90

			disease	like activities to protect cells from ROS cytotoxicity	
	Cu_xO@EM-K	GPx/CAT/SOD	Clearing peripheral amyloid-β associated with Alzheimer's disease	Scavenging H_2O_2 and synergizing with CAT- and SOD-like activities to mitigate Aβ-induced erythrocyte membrane oxidative damage	91
	$Cu_{5.4}O$ nanoparticles	GPx/CAT/SOD	Scavenging excessive ROS and alleviating inflammation-related diseases	Scavenging H_2O_2 and synergizing with SOD- and CAT-like activities to protect cells from ROS damage	92
	$Cu_{5.4}O$@Hep-PEG hydrogels	GPx/CAT/SOD	Inhibiting inflammation and promoting wound healing	Scavenging H_2O_2 and synergizing with CAT- and SOD-like activities to scavenge ROS from wound sites	93
	$PtCu_3$-PEG nanocages	GPx/POD	Depleting overexpressed GSH and enhancing sonodynamic tumor therapy	Depleting overexpressed GSH to decrease the scavenging of ROS in chemodynamic-enhanced sonodynamic cancer therapy	53
	Fe-CDs@Ang	GPx/CAT/OXD/POD/SOD/TPx	Activating autophagy-lysosome pathway for drug-resistant glioblastoma therapy	Depleting overexpressed GSH to make tumor cells more sensitive to the ROS changes	110
Fe	Fe-N/C SACs	GPx/CAT/OXD/POD	Protection of cells from oxidative stress by scavenging ROS	Scavenging H_2O_2 and regulating the concentration of H_2O_2 to deliver cellular signals	108
	$KCa(H_2O)_2[Fe^{III}(CN)_6]\cdot H_2O$ (CaPB)	GPx/CAT/POD/SOD	Regulating inflammation and inhibiting ferroptosis in acute kidney injury therapy	Scavenging H_2O_2 and synergizing with CAT- and SOD-like activities to effectively scavenge diverse RONS	111
	C-Mn_3O_4 nanoparticles	GPx	Passing the blood-brain barrier and treating Huntington's disease	Scavenging H_2O_2 and reducing the associated oxidative damage, thereby preventing the mitochondrial dysfunctions and concomitant redox imbalance	49
	HSA-Mn_3O_4	GPx/CAT/SOD	Alleviating reperfusion-induced nervous system damage in ischemic stroke	Scavenging H_2O_2 and synergizing with CAT- and SOD-like activities to effectively scavenge ROS	86
	$LiMn_2O_4$	GPx/CAT/SOD	Treating inflammatory bowel disease with a low dosage	Scavenging H_2O_2 and synergizing with CAT- and SOD-like activities to achieve self-cascading antioxidant activity and effectively scavenge ROS	89
Mn	MnO_2-BSA nanoparticles	GPx/CAT/OXD/POD/SOD	Protection of cells from oxidative stress by scavenging ROS	Scavenging H_2O_2	88
	Mn_3O_4 nanoflowers	GPx/CAT/SOD	Providing cytoprotection in Parkinson's disease	Scavenging H_2O_2 and fine-tuning the concentration of H_2O_2 for cell signaling	84
			Keeping NO bioavailability in human endothelial cells	Scavenging H_2O_2 and fine-tuning the concentration of H_2O_2 for cell signaling	52
	Mn_3O_4 in nanoform	GPx/CAT/SOD	Defending cells from oxidative stress by scavenging excess ROS	Scavenging H_2O_2 and fine-tuning the concentration of H_2O_2 for cell signaling	85
	Mn_3O_4 nanorods	GPx/CAT/POD/SOD	Scavenging excessive ROS and ameliorating Parkinson's disease	Scavenging H_2O_2 and synergizing with CAT- and SOD-like activities to effectively scavenge ROS	87
Mo	MoS_2	GPx/CAT/POD/SOD	Relieving hepatic fibrosis and suppressing inflammation	Scavenging H_2O_2 and synergizing with CAT- and SOD-like activities and constituting a self-cascade platform to inhibit ROS production	112
	MoO_3 nanowires	GPx	-	-	50

Pt	Au@Pt nanoparticles	GPx/Polyphenol oxidase /Lipoxygenase	-	-	113
	Janus BPQDs/Pt/AFSNs	GPx/CAT/OXD/POD/SOD	Scavenging excessive ROS and treating ROS-induced ear inflammation	Scavenging H_2O_2	114
Ru	Pt (IV)-Ru hybrid prodrug	GPx/CAT/POD	Alleviating tumor hypoxia, enhancing oxidative stress, and depleting GSH	Depleting overexpressed GSH to overcome cisplatin resistance	55
	RuO_2 nanoparticles	GPx/CAT/POD/SOD	Alleviating acute kidney injury	Scavenging H_2O_2 and synergizing with CAT- and SOD-like activities and exhibiting cytoprotective effect on oxidative stress-induced nephrotoxicity	115
Se	2D $MoSe_2$@PVP nanosheets	GPx/CAT/POD/SOD	Scavenging RONS heat-resistantly and alleviating acute pancreatitis	Scavenging H_2O_2 and synergizing with CAT- and SOD-like activities to effectively scavenge ROS	76
	Fe_2NC@Se nanoparticles	GPx/CAT/OXD/SOD	Inhibiting neural apoptosis after cerebral ischemia-reperfusion injury	Scavenging H_2O_2 and synergizing with CAT- and SOD-like activities to effectively scavenge ROS	73
	GO-Se nanocomposite	GPx	Protection of cells from oxidative stress by scavenging ROS	Scavenging H_2O_2 and protecting cells from ROS damage	43
	GO $(mPEGSe)_2$	GPx	Modulating the balance of ROS	Scavenging H_2O_2 and protecting cells from high ROS level	71
	HEP-SeNPs	GPx/CAT/SOD	Defending cells from oxidative stress by scavenging excess ROS	Scavenging H_2O_2 and synergizing with CAT- and SOD-like activities to effectively scavenge ROS	79
	Lf-Au-Bi_2Se_3 nanodots	GPx/CAT/POD/SOD	Passing the blood-brain barrier and treating Parkinson's disease	Scavenging H_2O_2 and synergizing with CAT- and SOD-like activities to alleviate ROS levels and ameliorate the mitochondrial state	74
	$MoSe_2$-PVP nanoparticles	GPx/CAT/POD/SOD	Scavenging RONS heat-resistantly and alleviating acute pancreatitis	Scavenging H_2O_2	75
	PEG-modified Mo_3Se_4 nanoflakes	GPx/CAT/POD/SOD	Inhibiting colitis by preventing oxidative damage and intestine barrier breakdown	Scavenging H_2O_2 and synergizing with CAT- and SOD-like activities to scavenge ROS and reconstitute of the Nrf2-mediated cellular anti-oxidative system	77
	MSe-HA nanoparticles	GPx	Treating local inflammation and sepsis injury simultaneously	Scavenging H_2O_2 and inhibiting the overexpression of pro-inflammatory cytokines	45
	PDASeCys	GPx/CAT/SOD	Treating Parkinson's disease	Scavenging H_2O_2 and synergizing with CAT- and SOD-like activities to effectively scavenge ROS	78
	Se-DG	GPx	Serving as a green catalyst in alkene epoxidation with H_2O_2	Supporting the ability to activate H_2O_2	120
	Se@Me@MnO_2	GPx/CAT/SOD	Resisting ROS-mediated damage and alleviating ear inflammation	Scavenging H_2O_2 and synergizing with CAT- and SOD-like activities to scavenge ROS	121
	Se@pDA	GPx	Alleviating lung inflammation and protecting cells against oxidative damage	Scavenging H_2O_2 effectively	44
	(Sec-Arg-Gly-Asp-Cys)-modified Au nanoparticles	GPx	-	-	59
	UiO-66-Se	GPx	-	-	72

	CuV_2O_6, MnV_2O_6, ZnV_2O_6	GPx	Increasing NO bioavailability and protecting cells from excessive ROS	Scavenging H_2O_2 and mediating the release of NO from S-nitrosothiols at physiological pH	51
	MIL-47(V)-X (X=F, Br, NH_2, CH_3, OH, and H)	GPx	Alleviating a broad-spectrum inflammation including ear injury and colitis	Scavenging H_2O_2 and inducing the M1 to M2 phenotypic polarization of macrophages	48
	$GdVO_4/Eu^{3+}$ nanoparticles	GPx	Exerting direct antioxidant effect and activating GSH signalling for anti-aging	Scavenging H_2O_2 and activating GSH signalling for anti-aging	81, 82
	VN_4 single-atom	GPx/CAT/POD	Accelerating the scalp healing from brain trauma	Scavenging H_2O_2 and lipid peroxides accumulated in the scalp following injuries	83
V	V_2O_5 nanosheets	GPx	Counteracting redox stress and blocking reactivation and replication of HIV-1	Scavenging H_2O_2, counteracting redox stress and blocking reactivation and replication of HIV-1	122
	V_2O_5 nanowires	GPx	Scavenging ROS and protecting cells from oxidative stress	Scavenging H_2O_2 and supplying the antioxidant system of the cell	39, 46
	V_2O_5@pDA@MnO_2	GPx/CAT/SOD	Alleviating ear inflammation and protecting cells against oxidative damage	Scavenging H_2O_2 and synergizing with CAT- and SOD-like activities to scavenge ROS	123
	2D V_2C MXenzyme	GPx/CAT/POD/SOD/TPx/Hydroperoxide lyase	Treating ROS-mediated inflammatory and neurodegenerative diseases Protecting nerves against ischemic stroke and serving for MR imaging	Scavenging H_2O_2 and maintaining appropriate H_2O_2 levels in cells	47 80
W	WS_2-PVP nanoflowers	GPx/CAT/SOD	Reducing inflammation caused by acute liver injury	Scavenging H_2O_2 and catalyzing GSH to reduce peroxide	118
Zn	ZnO	GPx/glycosidase	Catalysing the generation of NO from endogenous and exogenous prodrugs	Catalytically decomposing endogenous GSNO to generate NO	124
	BN-GDY	GPx/POD	Inhibiting colorectal cancer cell proliferation through attenuating tumor hypoxia	Depleting overexpressed GSH and hindering the GSH-induced ROS scavenging capacity	125
	CuFeP	GPx/POD	Depleting overexpressed GSH and enhancing oxidative stress for tumor therapy	Depleting overexpressed GSH to decrease the scavenging of ROS and improve •OH-medi-ated tumor therapy	58
	$CuFe_2O_4$@PEG	GPx/CAT/POD	Enhancing oxidative stress, reducing GSH, and alleviating tumor hypoxia	Depleting overexpressed GSH to decrease the scavenging of ROS and improve •OH-medi-ated tumor therapy	117
multiple active centers	IMOP	GPx/CAT	Relieving tumor hypoxia and depleting overexpressed GSH for tumor therapy	Depleting overexpressed GSH to decrease the scavenging of ROS	116
	$MnFe_2O_4$@MOF	GPx/CAT	Relieving tumor hypoxia and depleting overexpressed GSH for tumor therapy	Depleting overexpressed GSH to decrease the scavenging of ROS	56
	$SnFe_2O_4$	GPx/CAT	Relieving tumor hypoxia and depleting overexpressed GSH for tumor therapy	Depleting overexpressed GSH to decrease the scavenging of ROS and improve •OH- and $O_2^{\bullet-}$-medi-ated synergistic tumor therapy	57
	ZIF-67/$Cu_{0.76}Co_{2.24}O_4$ nanospheres	GPx/POD/SOD/laccase	Monitoring of 3,4-dihydroxyphenylacetic acid based on laccase-like activity	-	126
	O-NZ	GPx/SOD	Scavenging RONS and alleviating acute brain injury	Scavenging H_2O_2	127

Notes: (A) The “Active atom” and “Nanozyme” columns are listed in alphabetical order. (B) Organoselenium compounds, organotellurium compounds, and nanozymes obtained by combining them with supramolecular-assembled scaffolds are not listed. More information can be found in ref. 65.

Table 2 Kinetics parameters of GPx-like nanozymes

Active atom	Nanozyme	Substrate	K_m/mM	V_{max}/μM·min^{-1}	K_{cat}/s^{-1}	Experiential conditions	Ref.
Au	Au_{25} clusterzyme	H_2O_2		470		C(GSH) = 2 mM, C(NADPH) = 200 mM, C(GR) = 1.7 U·mL^{-1}, C(nanozyme) = 10 ng·μL^{-1}	103
	$Au_{24}Cd_1$ clusterzyme	H_2O_2		100			
	$Au_{24}Cu_1$ clusterzyme	H_2O_2		340			
Co	Co/PMCS	H_2O_2	0.26	17.44		25 °C, pH = 7.4, C(GSH) = 2 mM, C(NADPH) = 0.4 mM, C(GR) = 1.7 U, C(nanozyme) = 2.5 μM	107
		GSH	2.81	12.97		25 °C, pH = 7.4, C(H_2O_2) = 240 μM, C(NADPH) = 0.4 mM, C(GR) = 1.7 U, C(nanozyme) = 2.5 μM	
Cu	Cu nanoclusters (Cu NCs)	H_2O_2	0.097	6.781		37 °C, pH = 7.2, C(GSH) = 1 mM, C(DTNB) = 1 mM, C(nanozyme) = 20 μg·mL^{-1}	96
		GSH	0.913	4.766		37 °C, pH = 7.2, C(H_2O_2) = 1 mM, C(DTNB) = 1 mM, C(nanozyme) = 20 μg·mL^{-1}	
	Cu-TCPP MOF nanodots (CTMDs)	H_2O_2	0.199±0.12			25 °C, pH = 7.4, C(GSH) = 2 mM, C(NADPH) = 0.4 mM, C(GR) = 1.7 U, C(nanozyme) = 3.5 μg·mL^{-1} (with the Cu content)	95
		GSH	1.25±0.48			25 °C, pH = 7.4, C(H_2O_2) = 240 μM, C(NADPH) = 0.4 mM, C(GR) = 1.7 U, C(nanozyme) = 3.5 μg·mL^{-1} (with the Cu content)	
	CuO NP-POM	H_2O_2	0.15	7.806		pH = 7.4, C(GSH) = 1 mM, C(NADPH) = 0.1 mM, C(GR) = 2 μM, C(nanozyme) = 100 μg·mL^{-1}	94
		GSH	0.11	4.71		pH = 7.4, C(H_2O_2) = 1 mM, C(NADPH) = 0.1 mM, C(GR) = 2 μM, C(nanozyme) = 100 μg·mL^{-1}	

	Cu_xO nanoparticle clusters	H_2O_2	0.163	295		25 °C, pH = 7.4, C(GSH) = 2 mM, C(NADPH) = 200 μM, C(GR) = 1.7 U, C(nanozyme) = 20 μg·mL^{-1}	90
		GSH	1.89	188		25 °C, pH = 7.4, C(H_2O_2) = 500 μM, C(NADPH) = 200 μM, C(GR) = 1.7 U, C(nanozyme) = 20 μg·mL^{-1}	
Fe	Fe-CDs@Ang	H_2O_2	4.52	81.96		C (GSH) = 8.4 mM, C(NADPH) = 300 μM, C(nanozyme) = 100 μg·mL^{-1}	110
	C-Mn_3O_4 nanoparticles	H_2O_2	1.09±0.06	95±11	1.152±0.009	25 °C, pH = 7.4, C(GSH) = 2 mM, C(NADPH) = 400 μM, C(GR) = 1.7 U, C(nanozyme) = 1.3 μM	49
		GSH	1.36±0.09	64±8	0.779±0.005	25 °C, pH = 7.4, C(H_2O_2) = 240 μM, C(NADPH) = 400 μM, C(GR) = 1.7 U, C(nanozyme) = 1.3 μM	
	MnO_2-BSA nanoparticles	H_2O_2	0.15	4		C(GSH) = 2 mM, C(nanozyme) = 10 μg·mL^{-1}	88
		GSH	4.03	16		C(H_2O_2) = 2.5 mM, C(nanozyme) = 10 μg·mL^{-1}	
Mn	Mn_3O_4 nanoflowers	H_2O_2	0.196	56		25 °C, pH = 7.4, C(GSH) = 2 mM, C(NADPH) = 200 μM, C(GR) = 1.7 U, C(nanozyme) = 10 ng·μL^{-1}	84
		GSH	1.16	78		25 °C, pH = 7.4, C(H_2O_2) = 1 mM, C(NADPH) = 200 μM, C(GR) = 1.7 U, C(nanozyme) = 10 ng·μL^{-1}	
	Mn_3O_4 cubes	H_2O_2	0.989	18.2		25 °C, pH = 7.4, C(GSH) = 2 mM, C(NADPH) = 200 μM, C(GR) = 1.7 U, C(nanozyme) = 10 ng·μL^{-1}	52
	Mn_3O_4 polyhedrons	H_2O_2	2.845	16.9			
	Mn_3O_4 flakes	H_2O_2	0.431	39.1			
	Mn_3O_4 nanoflowers	H_2O_2	0.19	54.5			
	MoO_3 nanowires	H_2O_2	5.61±0.18	840.34±26.48		25 °C, pH = 7.4, C(GSH) = 2 mM, C(NADPH) = 0.2 mM, C(GR) = 1.7 U, C(nanozyme) = 20 μg·mL^{-1}	50
		GSH	3.06±0.03	323.62±3.09		25 °C, pH = 7.4, C(H_2O_2) = 200 μM, C(NADPH) = 0.2 mM, C(GR) = 1.7 U, C(nanozyme) = 20 μg·mL^{-1}	
Mo							

	MoS_2	H_2O_2	0.04	39.6	1.05×10^{-3}	C(GSH) = 2 mM, C(NADPH) = 0.4 mM, C(GR) = 1.7 U, C(nanozyme) = 100 μg·mL^{-1}	112
		GSH	1.68	56.4	1.50×10^{-3}	C(H_2O_2) = 240 μM, C(NADPH) = 0.4 mM, C(GR) = 1.7 U, C(nanozyme) = 100 μg·mL^{-1}	
Pt	Janus BPQDs/Pt/AFSNs	H_2O_2	0.076	990		pH = 7.4, C(GSH) = 2 mM, C(NADPH) = 0.4 mM, C(GR) = 1.7 U, C(nanozyme) = 10 μg·mL^{-1}	114
	Janus Pt/AFSNs	H_2O_2	0.11	920			
Ru	RuO_2 nanoparticles	H_2O_2	0.0172	47.0		C(GSH) = 2.0 mM, C(NADPH) = 200 μM, C(GR) = 2.0 U, C(nanozyme) = 20 μg·mL^{-1}	115
		GSH	0.870	65.1		C(H_2O_2) = 0.5 mM, C(NADPH) = 200 μM, C(GR) = 2.0 U, C(nanozyme) = 20 μg·mL^{-1}	
	Fe_2NC@Se nanoparticles	GSH	0.072	14.025		37 °C, pH = 7.4, C(H_2O_2) = 0.5 mM, C(NADPH) = 0.25 mM, C(GR) = 1.0 U·mL^{-1}	73
	GO-Se nanocomposite	H_2O_2	0.04	30		25 °C, pH = 7.4, C(GSH) = 2 mM, C(NADPH) = 0.4 mM, C(GR) = 1.7 U, C(nanozyme) = 0.01 mg·mL^{-1}	43
		GSH	0.72	49.2		25 °C, pH = 7.4, C(H_2O_2) = 240 μM, C(NADPH) = 0.4 mM, C(GR) = 1.7 U, C(nanozyme) = 0.01 mg·mL^{-1}	
	Lf-Au-Bi_2Se_3 nanodots	H_2O_2	0.61	1280		25 °C, pH = 7.4, C(GSH) = 2 mM, C(NADPH) = 200 μM, C(GR) = 1.7 U, C(nanozyme) = 10 μg·mL^{-1}	74
	MSe nanoparticles	H_2O_2	0.15772	27.36		25 °C, pH = 7.4, C(GSH) = 2 mM, C(NADPH) = 0.4 mM, C(GR) = 1.7 U, C(nanozyme) = 20 μg·mL^{-1}	45
	MSe-HA nanoparticles	H_2O_2	0.1598	26.81			
	Se NPs	H_2O_2	0.20059	13.51			
	PDASeCys	H_2O_2	1.37	87		25 °C, C(GSH) = 1.5 mM, C(NADPH) = 1.25 mM, C(GR) = 1 U, C(nanozyme) = 0.5 mg·mL^{-1}	78

		GSH	2.56	219.6		25 °C, C(H_2O_2) = 3 mM, C(NADPH) = 1.25 mM, C(GR) = 1 U, C(nanozyme) = 0.5 mg·mL^{-1}	
Se-DG	Se-DG-1	H_2O_2	0.2398±0.061	604.8±85.32		24 °C, pH = 7, C(GSH) = 4000 μM, C(NADPH) = 100 μM, C(GR) = 1.02 U	120
	Se-DG-2	H_2O_2	0.1448±0.0334	499.2±50.64			
	Se-DG-6	H_2O_2	0.0826±0.0174	446.6±32.82			
	Se-DG-1	GSH	0.3482±0.0216	241.8±2.52			
	Se-DG-2	GSH	0.3654±0.0263	249.6±3.12		24 °C, pH = 7, C(H_2O_2) = 100 μM, C(NADPH) = 100 μM, C(GR) = 1.02 U	
	Se-DG-6	GSH	0.7753±0.028	332.4±8.58			
(Sec-Arg-Gly-Asp -Cys)-modified Au nanoparticles	URGDC	H_2O_2	0.28		0.014		59
	MPC 1	H_2O_2	0.22		0.247	37 °C, pH = 7.0, C(GSH) = 1 mM, C(NADPH) = 0.25 mM, C(GR) = 1 U	
	MPC 2	H_2O_2	0.18		0.261		
	URGDC	GSH	0.72		0.014	37 °C, pH = 7.0, C(H_2O_2) = 0.5 mM, C(NADPH) = 0.25 mM, C(GR) = 1 U	
	MPC 1	GSH	0.64		0.247		
	MPC 2	GSH	0.32		0.261		
CuV_2O_6		H_2O_2	0.02383	156.25		25 °C, pH = 7.4, C(GSH) = 2 mM, C(NADPH) = 0.2 mM, C(GR) = 1.7 U, C(nanozyme) = 20 μg·mL^{-1}	51
MIL-47(V)-Br		H_2O_2	0.022	96		pH = 7.4, C(GSH) = 2 mM, C(NADPH) = 0.4 mM, C(GR) = 1.7 U	48
MIL-47(V)-CH_3		H_2O_2	0.010	84			
MIL-47(V)- F		H_2O_2	0.007	108			
MIL-47(V)-H		H_2O_2	0.018	42			
MIL-47(V)-NH_2		H_2O_2	0.003	114			
MIL-47(V)-OH		H_2O_2	0.027	66			
MIL-47(V)-Br		GSH	3.99	186			
MIL-47(V)-CH_3		GSH	1.71	150			
MIL-47(V)- F		GSH	3.70	216		pH = 7.4, C(H_2O_2) = 0.4 mM, C(NADPH) = 0.4 mM, C(GR) = 1.7 U	

MIL-47(V)-H	GSH	2.67	84			
MIL-47(V)-NH_2	GSH	2.85	210			
MIL-47(V)-OH	GSH	3.18	96			
VN_4 single-atom	H_2O_2	0.050	7.90	0.0535	pH = 7.4, C(GSH) = 2 mM, C(NADPH) = 200 μM, C(GR) = 1.7 U·mL^{-1}, C(nanozyme) = 3.8 μM	83
	GSH	1.31	8.55	0.1667	pH = 7.4, C(H_2O_2) = 0.2 mM, C(NADPH) = 200 μM, C(GR) = 1.7 U·mL^{-1}, C(nanozyme) = 3.8 μM	
V_2O_5 nanowires	H_2O_2	0.11	430	0.065	25 °C, pH = 7.4, C(GSH) = 2 mM, C(NADPH) = 0.4 mM, C(GR) = 1.7 U, C(nanozyme) = 0.020 mg·mL^{-1}	39
	GSH	2.22	830		25 °C, pH = 7.4, C(H_2O_2) = 240 μM, C(NADPH) = 0.4 mM, C(GR) = 1.7 U, C(nanozyme) = 0.020 mg·mL^{-1}	
V_2O_5 nanowires	H_2O_2	0.04±0.00	192.31±6.58		25 °C, pH = 7.4, C(GSH) = 2 mM, C(NADPH) = 0.2 mM, C(GR) = 1.7 U, C(nanozyme) = 20 μg·mL^{-1}	50
	GSH	1.28±0.06	279.3±18.2		25 °C, pH = 7.4, C(H_2O_2) = 200 μM, C(NADPH) = 0.2 mM, C(GR) = 1.7 U, C(nanozyme) = 20 μg·mL^{-1}	
V_2O_5 nanowires	H_2O_2	0.0444±0.0017	192.3±6.6		25 °C, pH = 7.4, C(GSH) = 2 mM, C(NADPH) = 0.2 mM, C(GR) = 1.7 U, C(nanozyme) = 20 ng·μL^{-1}	46
V_2O_5 nanosheets	H_2O_2	0.0573±0.0038	233.1±16.3			
V_2O_5 nanoflowers	H_2O_2	0.0925±0.0034	340.1±21.3			
V_2O_5 nanospheres	H_2O_2	0.1437±0.0023	458.7±19.6			
V_2O_5 nanowires	GSH	1.28±0.0612	279.3±18.2			
V_2O_5 nanosheets	GSH	3.425±0.1217	467.3±55.8		25 °C, pH = 7.4, C(H_2O_2) = 200 μM, C(NADPH) = 0.2 mM, C(GR) = 1.7 U, C(nanozyme) = 20 ng·μL^{-1}	
V_2O_5 nanoflowers	GSH	1.671±0.041	432.9±18.1			
V_2O_5 nanospheres	GSH	1.958±0.0633	602.4±40.3			
V_2O_5 ultrathin nanosheet	H_2O_2	0.1122±0.0038	476.2±34.1		25 °C, pH = 7.4, C(GSH) = 2 mM, C(NADPH) = 0.2 mM, C(GR) = 1.7 U, C(nanozyme) = 20 ng·μL^{-1}	122

multiple active centres	V_2O_5@pDA@MnO_2	H_2O_2	0.16	88	25 °C, pH = 7.4, C(GSH) = 2 mM, C(NADPH) = 0.4 mM, C(GR) = 1.7 U, C(nanozyme) = 0.0125 mg·mL^{-1}	123
		GSH	7.2	190	25 °C, pH = 7.4, C(H_2O_2) = 240 μM, C(NADPH) = 0.4 mM, C(GR) = 1.7 U, C(nanozyme) = 0.0125 mg·mL^{-1}	
	2D V_2C MXenzyme	H_2O_2	10.86	9600	C(GSH) = 8.4 mM, C(NADPH) = 300 μM	47
	ZIF-67/$Cu_{0.76}Co_{2.24}O_4$ nanospheres	H_2O_2	0.549	0.045	pH = 7.4, C(GSH) = 2 mM, C(NADPH) = 0.2 mM, C(GR) = 1.7 U, C(nanozyme) = 100 μg·mL^{-1}	126
		GSH	0.484	0.036	pH = 7.4, C(H_2O_2) = 1 mM, C(NADPH) = 0.2 mM, C(GR) = 1.7 U, C(nanozyme) = 100 μg·mL^{-1}	
	O-NZ	H_2O_2	0.8204	72.97	25 °C, pH = 7.4, C(GSH) = 2 mM, C(NADPH) = 200 μM, C(GR) = 1.7 U, C(nanozyme) = 2.5 μM	127
		GSH	0.8688	18.49	25 °C, pH = 7.4, C(H_2O_2) = 200 μM, C(NADPH) = 200 μM, C(GR) = 1.7 U, C(nanozyme) = 2.5 μM	

4. Applications of GPx-like nanozymes

GPx-like nanozymes, which maintain the ROS metabolic balance, have shown immense potential for the treatment of oxidative stress-related diseases in recent years (Table 1). Some representative applications are discussed in this section.

4.1 *In vitro* cytoprotection

Due to their excellent ability to scavenge H_2O_2, GPx-like nanozymes have been well demonstrated as cytoprotective agents. V_2O_5 nanowires with GPx-like activity were pioneering work on GPx-like nanozymes. In subsequent experiments, V_2O_5 nanowires were found to effectively internalize into cells through endocytosis (Fig. 10A), maintaining relatively low H_2O_2 levels even in the presence of either extrinsic H_2O_2 or intrinsic peroxide induced by $CuSO_4$ or 3-amino-1,2,4-triazole (3-AT) (Fig. 10B and C). Using allyl alcohol (AA) or buthionine sulfoximine (BSO), which depletes GSH, confirmed GSH's involvement in the elimination of H_2O_2 (Fig. 10B and C). In addition, V_2O_5 nanowires were shown to protect cells from damage caused by excess ROS by reducing lipid peroxidation, protein carbonylation, and DNA strand breaks. Moreover, V_2O_5 nanowires allowed H_2O_2 scavenging without interfering with natural antioxidant processes.[39] Other GPx-like nanozymes based on Se,[43, 79] Cu,[96] Mn,[85, 88] and Fe[108] have also been reported for cytoprotection. Some of them combined GPx-like activity with SOD- and CAT-like activities to reduce ROS-induced apoptosis. As an example, Qi and co-workers developed MnO_2 NPs with multiple enzyme-like activities that were able to scavenge H_2O_2, $O_2^{\bullet-}$, and $^{\bullet}OH$ simultaneously (Fig. 10D). Fig. 10E shows apoptosis-related proteins expressed on western blots, indicating that MnO_2 NPs could inhibit H_2O_2-induced apoptosis by reducing the expression of apoptotic proteins, such as cytochrome c (Cyt C), apoptotic protease-activating factor 1 (Apaf 1), and caspase-3.[88]

In addition to scavenging ROS, producing nitric oxide (NO), which may be depleted by ROS, is also essential for maintaining endothelial cell function. In a recent study, ZnO with GPx-like activity was found to decompose S-nitrosoglutathione catalytically to produce NO. NO-sensitive electrodes were used to characterize the production of NO, and ZnO was found to increase NO production sixfold and maintain this activity for half a year. Meanwhile, due to its glycosidase-like activity, ZnO could promote NO production from exogenous β-gal-NONOate, potentially contributing to sustained NO supply. Taking advantage of the NO-generating function, ZnO showed great promise in treating endothelial dysfunction and its associated cardiovascular disease.[124]

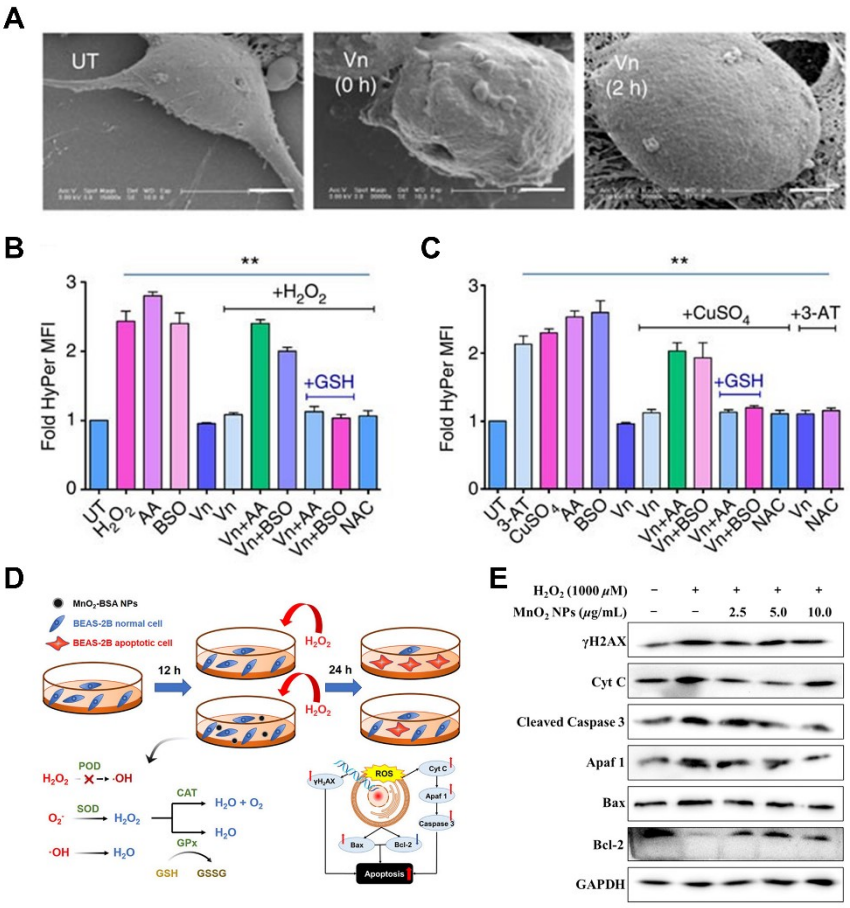

Fig. 10 (A) The SEM image of HEK293T cells with V_2O_5-untreated (UT), as well as V_2O_5-treated for 0 and 2 h. (B and C) The H_2O_2-scavaging ability of V_2O_5 under different treatments. Adapted with permission from ref. 39. Copyright (2014) Springer Nature. (D and E) MnO_2 NPs with multienzyme antioxidant activities and the cell protection effect and mechanism, as well as western blot expression of apoptosis-related proteins. Adapted with permission from ref. 88. Copyright (2022) American Chemical Society.

4.2 *In vivo* cytoprotection for anti-inflammation

When facing bacterial infection or other stimuli, macrophages could release inflammatory cytokines and generate ROS to clear the pathogen. A sustained inflammatory response, however, would overactivate macrophages, resulting in excessive ROS production and damage to cells and tissues. Therefore, GPx-like nanozymes possessing antioxidant properties have been extensively studied for their anti-inflammatory properties.[44, 45, 48] Since ROS contain not only H_2O_2, but also $O_2^{\bullet-}$, $^{\bullet}OH$, *etc*., GPx-like activity usually combined with other antioxidant enzyme-like activities, such as CAT, SOD, to mimic the natural antioxidative enzyme-based defense system. As an example, V_2O_5@pDA@MnO_2 was prepared using dopamine, which combined the GPx-like properties of V_2O_5 nanowires with the SOD and CAT-like properties of MnO_2 NPs. A synergistic antioxidative effect was demonstrated as shown in Fig. 11A, which catalyzed $O_2^{\bullet-}$ to O_2 and H_2O_2 with SOD-like activity, and then reduced H_2O_2 to H_2O with CAT- and GPx-like activities. As a result of *in vitro* oxidative stress induced by Rosup and *in vivo* phorbol 12-myristate 13-acetate (PMA)-induced ear inflammation in mice, it was found that V_2O_5@pDA@MnO_2 was efficiently able to scavenge ROS and alleviate inflammation.[123] The advantages of nanomaterials have recently led to the development of nanozymes, which possess multiple enzyme-like properties for treating inflammation.[93, 111, 112] For example, GPx-, CAT-, and SOD-like $Cu_{5.4}O$ NPs were found to be broad-spectrum anti-inflammatory agents in various inflammatory models, including acute liver injury, acute kidney injury (AKI) and diabetic wound healing.[92]

Aside from ROS, excessive reactive nitrogen species (RNS) like $^{\bullet}NO$ and peroxynitrite ($ONOO^-$) were also shown to contribute to inflammation. Sepsis, for example, is a condition that results in high morbidity and mortality due to the immoderate production of reactive oxygen and nitrogen species (RONS). At the beginning, the immune system was activated by pathogens and generated excessive H_2O_2 and HOCl in plasma. Due to its unique capability, H_2O_2 could enter cells easily and then not only participated in secondary reactions to produce $^{\bullet}OH$ but also activated nuclear transcription factor-κB, which stimulated the production of $^{\bullet}NO$, $O_2^{\bullet-}$, and $ONOO^-$. It has been discovered that Co single-atom catalysts (Co/PMCS) are capable of multiple enzyme-like activities that can be used to scavenge RONS in order to achieve desirable therapy efficacy. Through pyrolysis, Co/PMCS was produced, which mimicked SOD, GPx, and CAT to eliminate ROS, and also removed $^{\bullet}NO$ through the unoccupied Co-porphyrin center. According to *in vivo* experiments, Co/PMCS could significantly reduce RONS and pro-inflammatory cytokines in tissues, thereby mitigating inflammation. Treatment with Co/PMCS resulted in an increase in the 14-day survival rate of sepsis mice from 10% to 60%. Since H_2O_2 was critical in the redox mechanisms of sepsis, the GPx-like activity of Co/PMCS was possible to play a vital role in achieving the desirable therapy efficacy.[107] In addition, AKI and acute pancreatitis were associated with the over-production of RONS. As shown in Fig. 11B, ultrasmall CaPB synthesized with excellent RONS scavenging ability could cross the renal filtration threshold and prevent renal damage caused by AKI. The treatment of CaPB reduced the expression of pro-inflammatory cytokines TNF-α and IL-1β while enhancing the expression of anti-inflammatory cytokines IL-10. Further, CaPB could inhibit ferroptosis through elevated expression of GPx4, showing potential for clinical application.[111]

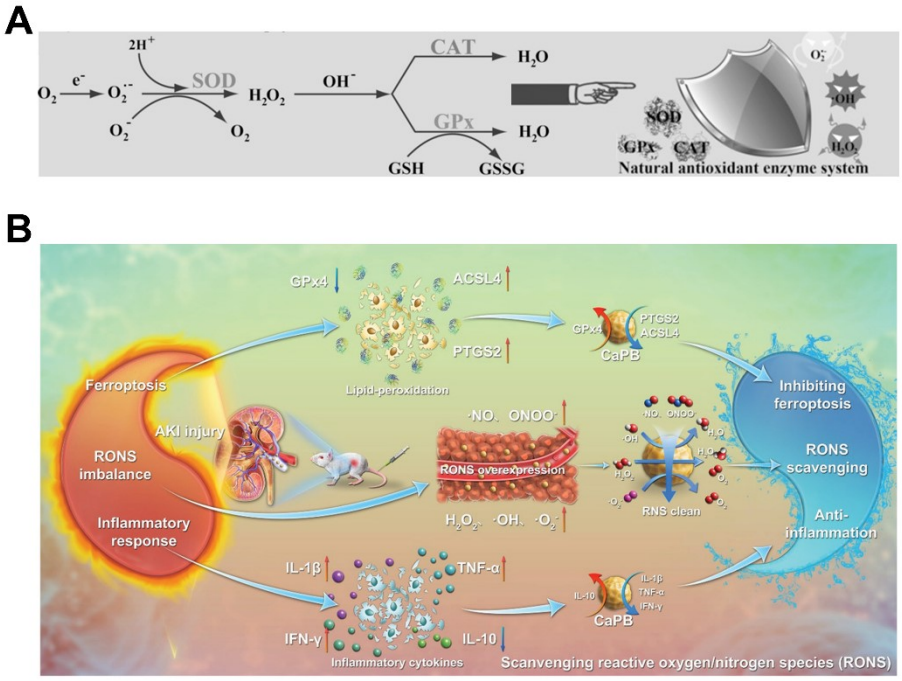

Fig. 11 (A) An illustration of V_2O_5@pDA@MnO_2 scavenging ROS. Adapted with permission from ref. 123. Copyright (2016) John Wiley and Sons. (B) Schematic illustration of CaPB nanozymes in the treatment of AKI. Adapted with permission from ref. 111. Copyright (2021) John Wiley and Sons.

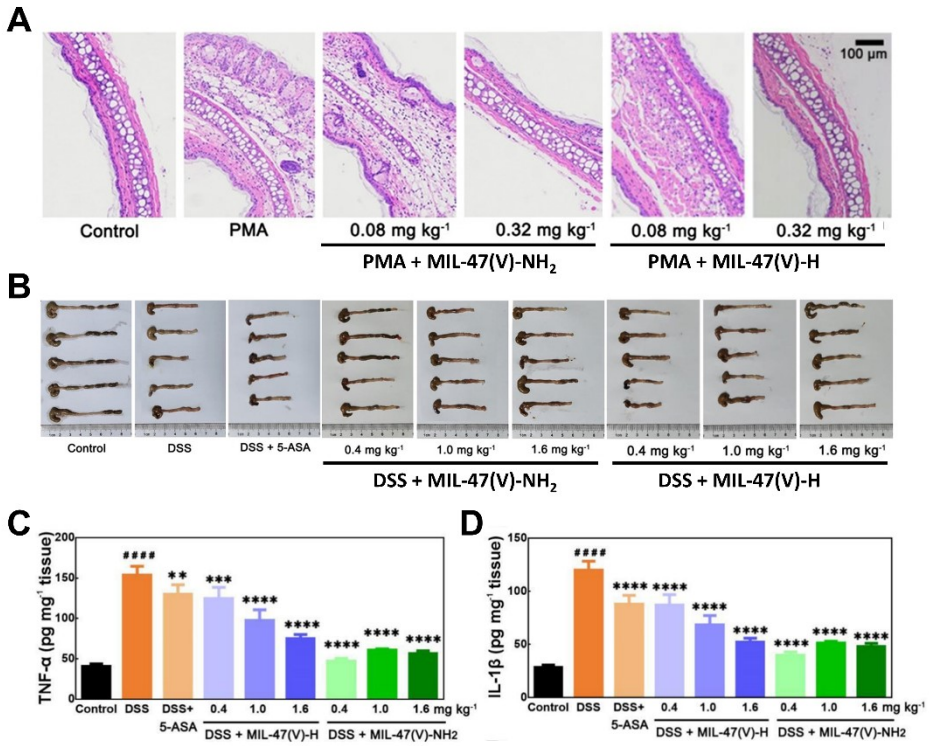

Fig. 12 (A) A comparison of hematoxylin and eosin-stained images of ear tissue with various treatments. (B) Colon images after various treatments. (C) TNF-α and (D) IL-1β levels in colon homogenates after different treatments. Adapted with permission from ref. 48. Copyright (2021) John Wiley and Sons.

H_2O_2 was considered to be among the most harmful ROS due to its longer life than $O_2^{\bullet-}$, its ease of diffusion across lipid membranes, as well as its precursor role in creating the highly harmful $^{\bullet}OH$. Therefore, several studies have focused on using GPx-like activity alone as an anti-inflammatory agent. Se NPs with GPx-like activity, for example, have been shown to effectively reduce inflammation. Moreover, their antioxidant coatings, such as pDA and hyaluronic acid, enhanced Se NPs' ROS scavenging ability.[44, 45] In contrast to Se NPs, Wei and co-workers synthesized MIL-47(V)-X MOF nanozymes with modulated GPx-like activity using a ligand engineering strategy (seeing Section 2.2). The most active MIL-47(V)-NH_2 was chosen for further anti-inflammation study, with the least active MIL-47(V)-H was also studied for comparison. As shown in Fig. 12A, PMA-induced ear inflammation was successfully developed with the ear swollen, and MIL-47(V) treatment alleviated this phenomenon. An additional dextran sulfate sodium (DSS)-induced colitis model was also treated with MIL-47(V) to demonstrate broad-spectrum anti-inflammation (Fig. 12B). With both recovered colon length and decreased inflammatory cytokines TNF-α and IL-1β (Fig. 12C and D), MIL-47(V) showed satisfactory therapeutic efficacy, even better than commercial drugs 5-aminosalicylic acid (5-ASA). In both models, MIL-47(V)-NH_2 with higher GPx-like activity demonstrated superior performance over MIL-47(V)-H, suggesting that the principles of structure-activity relationships might also guide the design of nanozyme-based therapeutics.[48]

4.3 *In vivo* cytoprotection for neuroprotection

Huntington's Disease (HD), Parkinson's Disease (PD), and Alzheimer's Disease (AD) are mainly caused by oxidative stress induced neuronal dysfunction in specific regions. HD, for example, is associated with deregulated GPx activity as well as consequent oxidative stress, and its main symptoms are motor impairments and cognitive and psychiatric alterations caused by lesions in the striatum of the brain. A study undertaken in 2013 suggested that supplementation of GPx activity could mitigate the toxicity of mutant huntingtin and ameliorate HD by decreasing ROS amount. Compared to other antioxidant enzyme activities, this neuroprotective effect was only shown for GPx, which was probably due to the fact that overexpression of GPx activity showed no inhibition effects on autophagy.[128] It is therefore possible to treat HD by introducing GPx-like nanozymes to replenish natural enzymes. GPx-like Mn_3O_4 with citrate functionalization (C-Mn_3O_4) was recently applied in treating 3-nitro propionic acid (3-NPA)-induced HD *in vivo*. The protective effect of C-Mn_3O_4 on neurons from 3-NPA-induced damage was found in several behavioral experiments, including motor function, anxiety-like behavior, depression-like behavior, and object recognition behavior (Fig. 13). Microscopic images of the cerebellum and basal ganglia also indicated a reduction in Huntington-like damage. Further experiment showed that C-Mn_3O_4 could provide GPx-like activity to scavenge H_2O_2 and reduce lipid peroxidation induced by 3-NPA. Benefiting from the overall decrease in oxidative distress, SOD and CAT activities also increased consequently. An analysis of mitochondrial parameters confirmed that C-Mn_3O_4 treatment could reduce the mitochondrial oxidative damage caused by 3-NPA, thus demonstrating its great therapeutic potential for HD.[49]

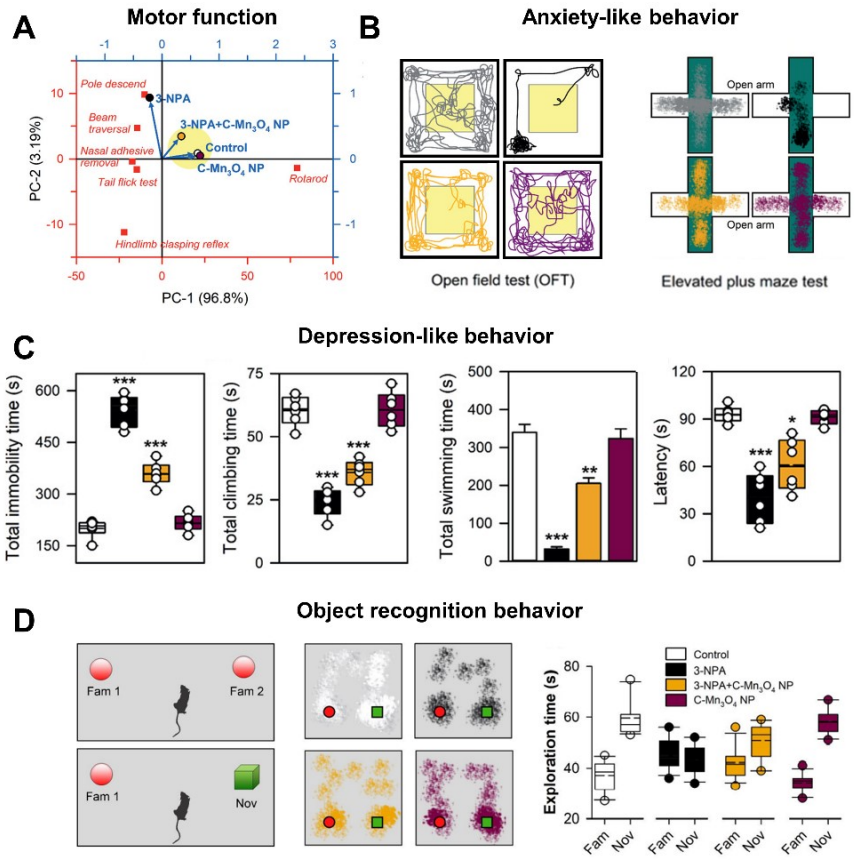

Fig. 13 (A) Principal component analysis considering all motor phenotypes. (B) Anxiety-like behavior evaluated by the open field test and elevated plus maze tests. (C) Depression-like behavior evaluated by immobility time, climbing time, swimming time, and latency to first immobility. (D) Object recognition behavior evaluated by the novel object recognition test, including the experimental setup, the movement pattern of the mice, and the novel object exploration time compared to the familiar one. Adapted with permission from ref. 49. Copyright (2021) John Wiley and Sons.

In contrast to HD, other neurodegenerative diseases lack direct links to GPx; therefore, GPx-like activity is usually combined with other antioxidant enzyme-like activities to achieve more comprehensive ROS scavenging. For example, Cu_xO nanozymes with SOD-, CAT-, and GPx-like activities were used in PD treatment to efficiently scavenge ROS, inhibit neurodegeneration, and improve memory.[90] An evaluation of the effectiveness of adding GPx-like activity concluded that adding extra GPx-like activity in combination with SOD- and CAT-like activities would increase neuronal cell activity by 30%, thereby improving the therapeutic efficacy.[78] If it comes to treating traumatic brain injury (TBI), the elimination of excessive $O_2^{\bullet-}$ and $^{\bullet}NO$ is more important. To treat TBI, an oligomeric nanozyme (O-NZ) based on N-doped graphite with active surface groups was synthesized. Carbogenic cores exhibited GPx- and SOD-like activities, and ultrafast electron transfer between the core and surface-active groups facilitated the high clearance of $^{\bullet}OH$, $O_2^{\bullet-}$, $^{\bullet}NO$, and $ONOO^-$. As a result of O-NZ's excellent ability to eliminate RONS, the survival rate of mice with acute brain trauma improved from 50 to 90% after one month, and long-term cognition was improved significantly.[127]

4.4 Tumor therapy

Unlike the above applications, ROS can effectively be harnessed to treat tumors. In tumor cells, however, GSH overexpression would reduce therapeutic efficacy by consuming ROS, such as $^{\bullet}OH$ and $^1O_2$. Therefore, GPx-like nanozymes were used in tumor therapies as auxiliary means of consuming GSH and thus in reducing ROS loss. For example, Shi, Fan, Yan, and co-workers synthesized ultrasmall Fe single-atom nanozymes (Fe-CDs), exhibiting six enzyme-like activities, including POD, oxidase (OXD), SOD, CAT, GPx, and thiol peroxidase (TPx). Due to the acidic environment of lysosomes, only POD- and OXD-like activities would be activated to produce toxic $^{\bullet}OH$ and $O_2^{\bullet-}$. As a result of these massive ROS, mitochondria would malfunction and apoptotic markers would be upregulated to trigger autophagy, leading to tumor cell death. Physiological pH is essential for SOD-, CAT-, GPx-, and TPx-like activities in early endosome, which regulate ROS to enhance autophagy and lysosome-based apoptosis. Specifically, SOD- and CAT-like activities converted $O_2^{\bullet-}$ to O_2 to alleviate hypoxia, while GPx and TPx-like activities consumed GSH to reduce ROS losses (Fig. 14A). Angiopep-2 was also used to modify Fe-CDs, which were called Fe-CDs@Ang, to improve their transport across the blood-brain barrier and selectively target glioblastoma. Further animal experiments showed that Fe-CDs@Ang were effective in

inhibiting glioma growth and improving the survival of mice with gliomas (Fig. 14B).[110]

As well as enhancing the effectiveness of ROS produced by POD- and OXD-like nanozymes, GPx-like nanozymes can also improve the efficacy of other therapeutic strategies. For example, $MnFe_2O_4$@MOF nanozymes with CAT- and GPx-like activities were synthesized for enhanced photodynamic therapy (Fig. 14C). As a photo sensitizer, $MnFe_2O_4$@MOF converted O_2 into $^1O_2$ under laser irradiation, thus resulting in obvious oxidative stress. The CAT-like activity could overcome hypoxia by continuously producing O_2 from endogenous H_2O_2. The GPx-like activity could deplete overexpressed GSH and generate a better photodynamic effect. Further experiments showed that the consumption of GSH by $MnFe_2O_4$@MOF itself effectively decrease $^1O_2$ depletion.[56] A similar effect was observed when $PtCu_3$ nanocages with GPx-like activity were used to consume GSH to enhance sonodynamic therapy, in which $^1O_2$ and •OH were generated under ultrasound. An *in vitro* experiment confirmed that GSH could be continuously depleted via a circular reaction in the presence of H_2O_2, thus weakening the capacity of tumor cells scavenging ROS by GSH and enhancing sonotoxicity (Fig. 14D).[53] Likewise, incorporating GPx- and CAT-like activities into chemotherapeutic drugs would provide a superior anticancer effect.[55] The GPx-like activity could deplete GSH and minimize GSH-medicated cisplatin detoxification. With nanomaterials' unique physicochemical properties, enzyme-like activities, such as POD, could be accelerated via photothermal effects. COF-909-Cu, for instance, possessed photothermal properties that enhanced the production of •OH and contributed to the chemodynamic therapy efficiency.[98] In another example, a simple $SnFe_2O_4$ nanozyme was used to combine photothermal, photodynamic, and chemodynamic therapies, resulting in significant tumor growth inhibition.[57] In both cases, GPx-like activity was responsible for reducing GSH levels.

4.5 Others

In addition to the examples mentioned above, GPx-like nanozymes have several other applications. According to Kavok and co-workers, orthovanadate nanoparticles that mimic GPx, such as $GdVO_4/Eu^{3+}$,[81, 82] were evaluated for their anti-aging effects on Wistar rats. Besides providing direct antioxidant effects, $GdVO_4/Eu^{3+}$ moderately inhibited the bioenergetic process and stimulated GSH turnover/regeneration, which declined with aging, thereby activating the GSH-dependent antioxidant system. In this way, $GdVO_4/Eu^{3+}$ will antioxidant defense and extend the health span. Additionally, GPx-like V_2O_5 nanozymes have been reported to inhibit human immunodeficiency virus (HIV-1) replication. By replenishing the impaired GPx activity and reducing H_2O_2 levels in infected cells, V_2O_5 nanozymes prevented HIV-1 reactivation by reducing the expression of genes, proinflammatory cytokines, and pro-apoptotic molecules involved in virus activation.[122]

Aside from therapeutic uses, GPx-like nanozymes could also be used for detection and epoxidation. A Fe^{2+} sensor based on GPx-like CuO-POM nanozymes was developed by Liu, Zhu, and co-workers. As *o*-phthalaldehyde reacted with GSH, a specific fluorescent isoindole derivative was formed, while the GPx-like activity consumed GSH as well, thus decreasing fluorescence. Since Fe^{2+} would recover fluorescence, a fluorometric sensor was constructed with a detection limit as low as 8.0 nM.[94] In addition, the selenium-doped graphite carbocatalyst also demonstrated GPx-like activity in epoxidating multiple aromatic and aliphatic alkene compounds, with ~90% conversion rate and ~75% epoxide yield.[120]

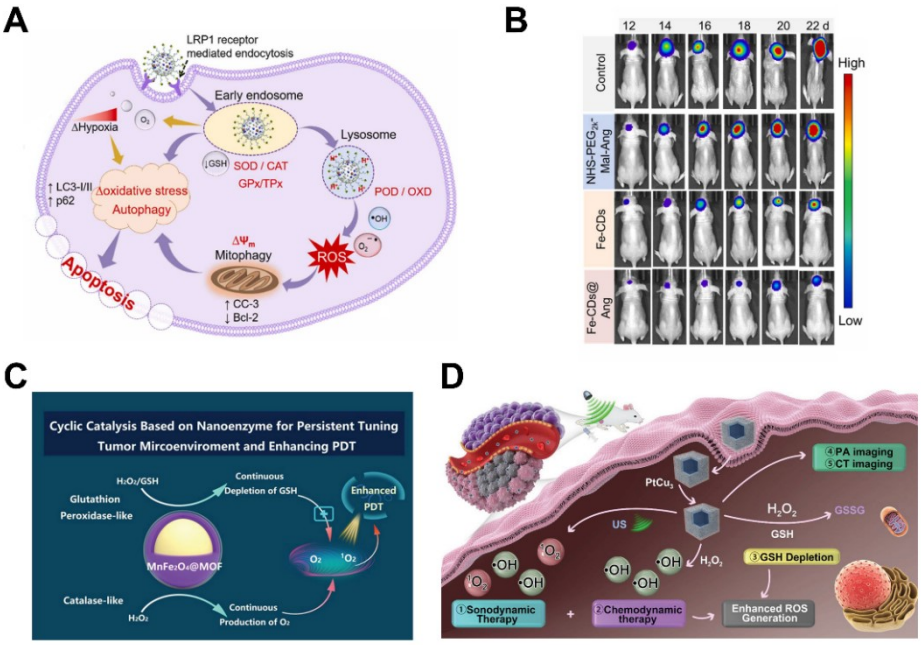

Fig. 14 (A) Induction of autophagy-lysosome pathways in tumor therapy by the Fe-CDs@Ang enzymatic cascade. (B) Bioluminescence images of mice with gliomas. Adapted with permission from ref. 110. Copyright (2022) Elsevier. (C) An illustration of $MnFe_2O_4$@MOF for tumor therapy. Reprinted with permission from ref. 56.

5. Conclusions and Prospects

The development of GPx mimics can be traced back nearly 40 years ago; however, the study of GPx-like nanozymes has not appeared until recently. It was the discovery of V_2O_5 nanowires mimicking GPx activity in 2014 that sparked interest in nanozymes with GPx-like activities. A growing amount of research has been conducted in the field of GPx-like nanozymes since then. This review summarizes the recent progress in the field of GPx-like nanozymes systematically and comprehensively. Starting from the mechanism of natural enzymes, the common catalytic mechanisms of GPx-like nanozymes are explored, followed by the classification of GPx-like nanozymes divided into Se-, V-, Mn-, Cu-based, and others based on their active centers, and their main applications in treating diseases caused by oxidative stress are also illustrated. In spite of the significant progress made on GPx-like nanozymes, many challenges remain to be addressed in the future.

(1) There is a lack of understanding of the structure-activity relationship and rational design methods of GPx-like nanozymes. GPx-like nanozyme research is currently largely based on screening and random synthesis. Meanwhile, the GPx-like activity is discovered along with other enzyme-like activities, hindering further understanding of the origin of GPx-like activity and its influencing factors. It is crucial for the success of future research in GPx-like nanozymes to have detailed findings regarding the structure-activity relationship. GPx-like nanozyme databases can be constructed using theoretical calculations, machine learning, and other methods along with experimental exploration to understand the relationship between enzyme activity and material properties. By doing so, it will be possible to design and develop highly active GPx-like nanozymes in a rational manner.

(2) There is not enough systematic analysis and in-depth research on GPx-like catalytic mechanisms and kinetics. To better understand catalytic reactions, it is essential to begin with understanding the internal mechanisms of GPx-like nanozymes. However, few studies have been conducted to fully understand the dynamics and mechanism of GPx-like nanozymes. The identification and characterization of active components, changes in the valence state of active site elements, and identification of intermediates in catalytic processes have not been thoroughly investigated. To explore more detailed catalytic mechanisms, practical theoretical computational methods as well as experimental techniques are needed, which is of great significance for future design and rational application.

(3) Research using GPx-like activity alone for biomedical treatment is relatively limited. A majority of bioapplications relies on multiple enzyme-like activities, with GPx-like activity only acting as an auxiliary component. It has been shown that, however, in some bioapplications, such as anti-inflammation, the nanozymes can still exert the necessary effect even when there is merely GPx-like activity. It may be possible, therefore, to conduct more in-depth research on biological mechanisms and to understand the differences between multienzyme-like activities and only GPx-like activity in disease therapy, in addition to treating with only GPx-like nanozymes in the future. GPx-like nanozymes will benefit from these in-depth investigations in the future when developed for biomedical applications.

(4) Despite the success of GPx-like nanozymes in biomedical applications, their biosafety, potential toxicity, and pharmacokinetics remain the main obstacles to clinical application. Currently, nanozymes' overall toxicity assessment, *in vivo* applicability, *in vivo* metabolic issues, and clinical adverse effects have not been sufficiently investigated. More attention should be paid to future research that encompasses everything from therapeutic modalities to toxicity assessments in pre-clinical trials. In order to improve the biosafety and increase the clinical translation potential of nanozymes, future research should correlate nanomaterial features and manufacturing procedures with their safety properties.

Conflicts of interest

There are no conflicts to declare.

Acknowledgements

This work is supported by the National Natural Science Foundation of China under Grant No. 22104054.

References

1 W. Droge, *Physiol. Rev.*, 2002, **82**, 47−95.
2 H. Sies and D. P. Jones, *Nat. Rev. Mol. Cell Biol.*, 2020, **21**, 363−383.
3 S. J. Forrester, D. S. Kikuchi, M. S. Hernandes, Q. Xu and K. K. Griendling, *Circul. Res.*, 2018, **122**, 877−902.
4 M. Valko, D. Leibfritz, J. Moncol, M. T. Cronin, M. Mazur and J. Telser, *Int. J. Biochem. Cell Biol.*, 2007, **39**, 44−84.
5 B. Yang, Y. Chen and J. Shi, *Chem. Rev.*, 2019, **119**, 4881−4985.
6 R. Mittler, S. Vanderauwera, N. Suzuki, G. Miller, V. B. Tognetti, K. Vandepoele, M. Gollery, V. Shulaev and F. Van Breusegem, *Trends Plant Sci.*, 2011, **16**, 300−309.
7 J. Li, F. Cao, H. L. Yin, Z. J. Huang, Z. T. Lin, N. Mao, B. Sun and G. Wang, *Cell Death & Disease*, 2020, **11**, 88.
8 R. Mittler, *Trends Plant Sci.*, 2017, **22**, 11−19.
9 T. Finkel and N. J. Holbrook, *Nature*, 2000, **408**, 239−247.
10 P. R. Angelova, N. Esteras and A. Y. Abramov, *Med. Res. Rev.*, 2021, **41**, 770−784.
11 M. T. Lin and M. F. Beal, *Nature*, 2006, **443**, 787−795.
12 S. Reuter, S. C. Gupta, M. M. Chaturvedi and B. B. Aggarwal, *Free Radical Biol. Med.*, 2010, **49**, 1603−1616.
13 H. Cai and D. G. Harrison, *Circul. Res.*, 2000, **87**, 840−844.
14 C. Iacobini, M. Vitale, C. Pesce, G. Pugliese and S. Menini, *Antioxidants*, 2021, **10**, 727.
15 H. Sies, *Exp. Physiol.*, 1997, **82**, 291−295.
16 C. J. Weydert and J. J. Cullen, *Nat. Protoc.*, 2010, **5**, 51−66.

17 G. C. Mills, *J. Biol. Chem.*, 1957, **229**, 189−197.
18 L. Flohe, W. A. Günzler and H. H. Schock, *FEBS Lett.*, 1973, **32**, 132−134.
19 J. T. Rotruck, A. L. Pope, H. E. Ganther, A. B. Swanson, D. G. Hafeman and W. G. Hoekstra, *Science*, 1973, **179**, 588−590.
20 O. Epp, R. Ladenstein and A. Wendel, *Eur. J. Biochem.*, 1983, **133**, 51−69.
21 F. Ursini, M. Maiorino, R. Brigelius-Flohé, K. D. Aumann, A. Roveri, D. Schomburg and L. Flohé, *Methods Enzymol.*, 1995, **252**, 38−53.
22 Y. Lin, J. Ren and X. Qu, *Acc. Chem. Res.*, 2014, **47**, 1097−1105.
23 D. Jiang, D. Ni, Z. T. Rosenkrans, P. Huang, X. Yan and W. Cai, *Chem. Soc. Rev.*, 2019, **48**, 3683−3704.
24 I. Di Leo, F. Messina, V. Nascimento, F. G. Nacca, D. Pietrella, E. J. Lenardão, G. Perin and L. Sancineto, *Mini-Rev. Org. Chem.*, 2019, **16**, 589−601.
25 A. Muller, E. Cadenas, P. Graf and H. Sies, *Biochem. Pharmacol.*, 1984, **33**, 3235−3239.
26 H. Sies, *Free Radical Biol. Med.*, 1993, **14**, 313−323.
27 T. Schewe, *Gen. Pharmacol.*, 1995, **26**, 1153−1169.
28 H. Sies and M. J. Parnham, *Free Radical Biol. Med.*, 2020, **156**, 107−112.
29 J. Zhang, L. Yang, Y. Wang, T. Cao, Z. Sun, J. Xu, Y. Liu and G. Chen, *ACS Appl. Bio Mater.*, 2021, **4**, 2217−2230.
30 M. R. Detty and S. L. Gibson, *Organometallics*, 1992, **11**, 2147−2156.
31 Y. Huang, J. Ren and X. Qu, *Chem. Rev.*, 2019, **119**, 4357−4412.
32 M. Liang and X. Yan, *Acc. Chem. Res.*, 2019, **52**, 2190−2200.
33 D. Li, Q. Xiong, L. Liang and H. Duan, *Biomater. Sci.*, 2021, **9**, 7323−7342.
34 Y. Li and J. Liu, *Mater. Horiz.*, 2021, **8**, 336−350.
35 W. Yang, X. Yang, L. Zhu, H. Chu, X. Li and W. Xu, *Coord. Chem. Rev.*, 2021, **448**, 214170.
36 J. Wu, X. Wang, Q. Wang, Z. Lou, S. Li, Y. Zhu, L. Qin and H. Wei, *Chem. Soc. Rev.*, 2019, **48**, 1004−1076.
37 M. Chang, C. Dong, H. Huang, L. Ding, W. Feng and Y. Chen, *Adv. Funct. Mater.*, 2022, **32**, 2204791.
38 G. Tang, J. He, J. Liu, X. Yan and K. Fan, *Exploration*, 2021, **1**, 75−89.
39 A. A. Vernekar, D. Sinha, S. Srivastava, P. U. Paramasivam, P. D'Silva and G. Mugesh, *Nat. Commun.*, 2014, **5**, 5301.
40 L. Flohé, G. Loschen, W. A. Gunzler and E. Eichele, *Hoppe-Seyler's Z. Physiol. Chem.*, 1972, **353**, 987−999.
41 M. A. Carsol, I. Pouliquen-Sonaglia, G. Lesgards, G. Marchis-Mouren, A. Puigserver and M. Santimone, *Eur. J. Biochem.*, 1997, **247**, 248−255.
42 R. Brigelius-Flohé and M. Maiorino, *Biochim. Biophys. Acta*, 2013, **1830**, 3289−3303.
43 Y. Huang, C. Liu, F. Pu, Z. Liu, J. Ren and X. Qu, *Chem. Commun.*, 2017, **53**, 3082−3085.
44 Y. Huang, Z. Liu, C. Liu, Y. Zhang, J. Ren and X. Qu, *Chem. – Eur. J.*, 2018, **24**, 10224−10230.
45 X. Chen, X. Zhu, Y. Gong, G. Yuan, J. Cen, Q. Lie, Y. Hou, G. Ye, S. Liu and J. Liu, *Appl. Mater. Today*, 2021, **22**, 100929.
46 S. Ghosh, P. Roy, N. Karmodak, E. D. Jemmis and G. Mugesh, *Angew. Chem. Int. Ed.*, 2018, **57**, 4510−4515.
47 W. Feng, X. Han, H. Hu, M. Chang, L. Ding, H. Xiang, Y. Chen and Y. Li, *Nat. Commun.*, 2021, **12**, 2203.
48 J. Wu, Y. Yu, Y. Cheng, C. Cheng, Y. Zhang, B. Jiang, X. Zhao, L. Miao and H. Wei, *Angew. Chem. Int. Ed.*, 2021, **60**, 1227−1234.
49 A. Adhikari, S. Mondal, M. Das, P. Biswas, U. Pal, S. Darbar, S. S. Bhattacharya, D. Pal, T. Saha-Dasgupta, A. K. Das, A. K. Mallick and S. K. Pal, *Adv. Healthcare Mater.*, 2021, **10**, 2001736.
50 S. Ghosh, S. Prasad and G. Mugesh, *Inorg. Chim. Acta*, 2019, **484**, 283−290.
51 S. Ghosh, P. Roy, S. Prasad and G. Mugesh, *Faraday Discuss.*, 2022, **234**, 284−303.
52 N. Singh, M. Geethika, S. M. Eswarappa and G. Mugesh, *Chem. – Eur. J.*, 2018, **24**, 8393−8403.
53 X. Zhong, X. Wang, L. Cheng, Y. a. Tang, G. Zhan, F. Gong, R. Zhang, J. Hu, Z. Liu and X. Yang, *Adv. Funct. Mater.*, 2019, **30**, 1907954.
54 W. Zeng, M. Yu, T. Chen, Y. Liu, Y. Yi, C. Huang, J. Tang, H. Li, M. Ou, T. Wang, M. Wu and L. Mei, *Adv. Sci.*, 2022, **9**, 2201703.
55 G. Yang, X. Su, B. Liang, Z. Pan, Q. Cao and Z. Mao, *Chem. Sci.*, 2022, **13**, 11360−11367.
56 S. Y. Yin, G. Song, Y. Yang, Y. Zhao, P. Wang, L. M. Zhu, X. Yin and X. B. Zhang, *Adv. Funct. Mater.*, 2019, **29**, 1901417.
57 L. Feng, B. Liu, R. Xie, D. Wang, C. Qian, W. Zhou, J. Liu, D. Jana, P. Yang and Y. Zhao, *Adv. Funct. Mater.*, 2020, **31**, 2006216.
58 X. Zhao, S. Yao, X. Wan, T. Huang, Z. Zhang, X. Wang, S. Wang, Q. Liang, Z. Li and L. Li, *Appl. Mater. Today*, 2021, **25**, 101255.
59 D. Zhang, N. Shen, J. Zhang, J. Zhu, Y. Guo and L. Xu, *RSC Adv.*, 2020, **10**, 8685−8691.
60 G. Mugesh and H. B. Singh, *Chem. Soc. Rev.*, 2000, **29**, 347−357.
61 K. P. Bhabak and G. Mugesh, *Acc. Chem. Res.*, 2010, **43**, 1408−1419.
62 E. E. Alberto, V. Nascimento and A. L. Braga, *J. Braz. Chem. Soc.*, 2010, **21**, 2032−2041.
63 Y. Huang, E. Su, J. Ren and X. Qu, *Nano Today*, 2021, **38**, 101205.
64 X. Huang, Y. Yin and J. Liu, *Macromol. Biosci.*, 2010, **10**, 1385−1396.
65 X. Huang, X. Liu, Q. Luo, J. Liu and J. Shen, *Chem. Soc. Rev.*, 2011, **40**, 1171−1184.
66 C. Hou, Q. Luo, J. Liu, L. Miao, C. Zhang, Y. Gao, X. Zhang, J. Xu, Z. Dong and J. Liu, *ACS Nano*, 2012, **6**, 8692−8701.
67 L. Miao, Q. Fan, L. Zhao, Q. Qiao, X. Zhang, C. Hou, J. Xu, Q. Luo and J. Liu, *Chem. Commun.*, 2016, **52**, 4092−4095.
68 X. Huang, Y. Yin, X. Jiang, Y. Tang, J. Xu, J. Liu and J. Shen, *Macromol. Biosci.*, 2009, **9**, 1202−1210.
69 X. Huang, Y. Yin, Y. Tang, X. Bai, Z. Zhang, J. Xu, J. Liu and J. Shen, *Soft Matter*, 2009, **5**, 1905−1911.
70 H. Zou, H. Sun, L. Wang, L. Zhao, J. Li, Z. Dong, Q. Luo, J. Xu and J. Liu, *Soft Matter*, 2016, **12**, 1192−1199.
71 J. Xia, F. Li, S. Ji and H. Xu, *ACS Appl. Mater. Interfaces*, 2017, **9**, 21413−21421.
72 W. Zhou, H. Li, B. Xia, W. Ji, S. Ji, W. Zhang, W. Huang, F. Huo and H. Xu, *Nano Res.*, 2018, **11**, 5761−5768.
73 R. Tian, H. Ma, W. Ye, Y. Li, S. Wang, Z. Zhang, S. Liu, M. Zang, J. Hou, J. Xu, Q. Luo, H. Sun, F. Bai, Y. Yang and J. Liu, *Adv. Funct. Mater.*, 2022, **32**, 2204025.
74 L. Li, Y. Lu, X. Xu, X. Yang, L. Chen, C. Jiang, Y. Wang, W. Hu,

X. Wei and Z. Yang, *Adv. Healthcare Mater.*, 2021, **10**, 2100316.
75 P. Xie, L. Zhang, H. Shen, H. Wu, J. Zhao, S. Wang and L. Hu, *J. Nanobiotechnol.*, 2022, **20**, 113.
76 L. Zhang, P. Xie, H. Wu, J. Zhao and S. Wang, *Chem. Eng. J.*, 2022, **446**, 136792.
77 H. Guo, H. Guo, Y. Xie, Y. Chen, C. Lu, Z. Yang, Y. Zhu, Y. Ouyang, Y. Zhang and X. Wang, *Redox Biol.*, 2022, **56**, 102441.
78 W. Wang, J. Zheng, H. Zhou, Q. Liu, L. Jia, X. Zhang, D. Ge, W. Shi and Y. Sun, *ACS Appl. Mater. Interfaces*, 2022, **14**, 32901−32913.
79 H. He, C. Liu, C. Shao, Y. Wu and Q. Huang, *Mater. Lett.*, 2022, **317**, 132079.
80 H. Hu, H. Huang, L. Xia, X. Qian, W. Feng, Y. Chen and Y. Li, *Chem. Eng. J.*, 2022, **440**, 135810.
81 Y. V. Nikitchenko, V. K. Klochkov, N. S. Kavok, N. A. Karpenko, S. L. Yefimova, I. V. Nikitchenko and A. I. Bozhkov, *Biol. Trace Elem. Res.*, 2021, **199**, 649-659.
82 Y. V. Nikitchenko, V. K. Klochkov, N. S. Kavok, K. A. Averchenko, N. A. Karpenko, I. V. Nikitchenko, S. L. Yefimova and A. I. Bozhkov, *Biol. Trace Elem. Res.*, 2021, **199**, 4183−4192.
83 S. Zhang, Y. Li, S. Sun, L. Liu, X. Mu, S. Liu, M. Jiao, X. Chen, K. Chen, H. Ma, T. Li, X. Liu, H. Wang, J. Zhang, J. Yang and X. D. Zhang, *Nat. Commun.*, 2022, **13**, 4744.
84 N. Singh, M. A. Savanur, S. Srivastava, P. D'Silva and G. Mugesh, *Angew. Chem. Int. Ed.*, 2017, **56**, 14267−14271.
85 N. Singh, M. A. Savanur, S. Srivastava, P. D'Silva and G. Mugesh, *Nanoscale*, 2019, **11**, 3855−3863.
86 G. Huang, J. Zang, L. He, H. Zhu, J. Huang, Z. Yuan, T. Chen and A. Xu, *ACS Nano*, 2021, **16**, 431−452.
87 Z. Xu, A. Qu, W. Wang, M. Lu, B. Shi, C. Chen, C. Hao, L. Xu, M. Sun, C. Xu and H. Kuang, *Adv. Healthcare Mater.*, 2021, **10**, 2101316.
88 Y. Zhang, L. Chen, R. Sun, R. Lv, T. Du, Y. Li, X. Zhang, R. Sheng and Y. Qi, *ACS Biomater. Sci. Eng.*, 2022, **8**, 638−648.
89 Q. Wang, C. Cheng, S. Zhao, Q. Liu, Y. Zhang, W. Liu, X. Zhao, H. Zhang, J. Pu, S. Zhang, H. Zhang, Y. Du and H. Wei, *Angew. Chem. Int. Ed.*, 2022, **61**, e202201101.
90 C. Hao, A. Qu, L. Xu, M. Sun, H. Zhang, C. Xu and H. Kuang, *J. Am. Chem. Soc.*, 2019, **141**, 1091−1099.
91 M. Ma, Z. Liu, N. Gao, Z. Pi, X. Du, J. Ren and X. Qu, *J. Am. Chem. Soc.*, 2020, **142**, 21702−21711.
92 T. Liu, B. Xiao, F. Xiang, J. Tan, Z. Chen, X. Zhang, C. Wu, Z. Mao, G. Luo, X. Chen and J. Deng, *Nat. Commun.*, 2020, **11**, 2788.
93 Y. Peng, D. He, X. Ge, Y. Lu, Y. Chai, Y. Zhang, Z. Mao, G. Luo, J. Deng and Y. Zhang, *Bioact. Mater.*, 2021, **6**, 3109−3124.
94 Y. Xu, P. Li, X. Hu, H. Chen, Y. Tang, Y. Zhu, X. Zhu, Y. Zhang, M. Liu and S. Yao, *ACS Appl. Nano Mater.*, 2021, **4**, 8302−8313.
95 L. Zhang, Y. Zhang, Z. Wang, F. Cao, Y. Sang, K. Dong, F. Pu, J. Ren and X. Qu, *Mater. Horiz.*, 2019, **6**, 1682−1687.
96 Y. Peng, Y. Ren, H. Zhu, Y. An, B. Chang and T. Sun, *RSC Adv.*, 2021, **11**, 14517−14526.
97 L. Zhang, Y. Xiao, Q. C. Yang, L. L. Yang, S. C. Wan, S. Wang, L. Zhang, H. X. Deng and Z. J. Sun, *Adv. Funct. Mater.*, 2022, **32**, 2201542.
98 L. Zhang, Q. C. Yang, S. Wang, Y. Xiao, S. C. Wan, H. Deng and Z. J. Sun, *Adv. Mater.*, 2022, **34**, 2108174.
99 X. Huang, Z. Dong, J. Liu, S. Mao, G. Luo and J. Shen, *Macromol. Rapid Commun.*, 2006, **27**, 2101−2106.
100 Y. Yin, S. Jiao, C. Lang and J. Liu, *RSC Adv.*, 2014, **4**, 25040−25050.
101 Y. Yin, S. Jiao, C. Lang and J. Liu, *Soft Matter*, 2014, **10**, 3374−3385.
102 S. Yu, W. Zhang, J. Zhu, Y. Yin, H. Jin, L. Zhou, Q. Luo, J. Xu and J. Liu, *Macromol. Biosci.*, 2011, **11**, 821−827.
103 H. Liu, Y. Li, S. Sun, Q. Xin, S. Liu, X. Mu, X. Yuan, K. Chen, H. Wang, K. Varga, W. Mi, J. Yang and X. D. Zhang, *Nat. Commun.*, 2021, **12**, 114.
104 S. Sun, H. Liu, Q. Xin, K. Chen, H. Ma, S. Liu, X. Mu, W. Hao, S. Liu, Y. Gao, Y. Wang, J. Pei, R. Zhao, S. Zhang, X. Zhang, H. Wang, Y. Li and X. D. Zhang, *Nano Lett.*, 2021, **21**, 2562−2571.
105 R. Yan, S. Sun, J. Yang, W. Long, J. Wang, X. Mu, Q. Li, W. Hao, S. Zhang, H. Liu, Y. Gao, L. Ouyang, J. Chen, S. Liu, X. D. Zhang and D. Ming, *ACS Nano*, 2019, **13**, 11552−11560.
106 S. Zhang, Y. Liu, S. Sun, J. Wang, Q. Li, R. Yan, Y. Gao, H. Liu, S. Liu, W. Hao, H. Dai, C. Liu, Y. Sun, W. Long, X. Mu and X. D. Zhang, *Theranostics*, 2021, **11**, 2806−2821.
107 F. Cao, L. Zhang, Y. You, L. Zheng, J. Ren and X. Qu, *Angew. Chem. Int. Ed.*, 2020, **59**, 5108−5115.
108 M. Lu, C. Wang, Y. Ding, M. Peng, W. Zhang, K. Li, W. Wei and Y. Lin, *Chem. Commun.*, 2019, **55**, 14534−14537.
109 H. Liu, J. Wang, C. Song, K. Zhou, B. Yu, J. Jiang, J. Qian, X. Zhang and H. Wang, *ACS Appl. Mater. Interfaces*, 2022, **14**, 29650−29658.
110 P. Muhammad, S. Hanif, J. Li, A. Guller, F. U. Rehman, M. Ismail, D. Zhang, X. Yan, K. Fan and B. Shi, *Nano Today*, 2022, **45**, 101530.
111 K. Wang, Y. Zhang, W. Mao, W. Feng, S. Lu, J. Wan, X. Song, Y. Chen and B. Peng, *Adv. Funct. Mater.*, 2021, **32**, 2109221.
112 X. Zhang, S. Zhang, Z. Yang, Z. Wang, X. Tian and R. Zhou, *Nanoscale*, 2021, **13**, 12613−12622.
113 J. W. Lee, S. Yoon, Y. M. Lo, H. Wu, S. Y. Lee and B. Moon, *RSC Adv.*, 2015, **5**, 63757−63764.
114 S. Zhang, J. Chen, M. L. Lian, W. S. Yang and X. Chen, *Chem. Eng. J.*, 2022, **446**, 136794.
115 Z. Liu, L. Xie, K. Qiu, X. Liao, T. W. Rees, Z. Zhao, L. Ji and H. Chao, *ACS Appl. Mater. Interfaces*, 2020, **12**, 31205−31216.
116 M. Li, L. Huo, J. Zeng, G. Zhu, S. Shi, X. Liu, X. Zhu, G. Huang, D. Qiu, J. Jia, K. Ni and Z. Zhao, *Chem. Eng. J.*, 2022, **440**, 135966.
117 S. Li, H. Ding, J. Chang, S. Dong, B. Shao, Y. Dong, S. Gai, F. He and P. Yang, *J. Colloid Interface Sci.*, 2022, **623**, 787−798.
118 H. Xu, Z. Zhang, L. Zhang, Z. Chen and S. Wang, *J. Colloid Interface Sci.*, 2022, **625**, 544−554.
119 S. Dong, Y. Dong, T. Jia, S. Liu, J. Liu, D. Yang, F. He, S. Gai, P. Yang and J. Lin, *Adv. Mater.*, 2020, **32**, 2002439.
120 S. Maity and B. B. Dhar, *Catal. Sci. Technol.*, 2022, **12**, 1296−1312.
121 Y. Ai, J. You, J. Gao, J. Wang, H. Sun, M. Ding and Q. Liang, *Nano Res.*, 2021, **14**, 2644−2653.
122 S. Singh, S. Ghosh, V. K. Pal, M. Munshi, P. Shekar, D. T. Narasimha Murthy, G. Mugesh and A. Singh, *EMBO Mol. Med.*, 2021, **13**, e13314.
123 Y. Huang, Z. Liu, C. Liu, E. Ju, Y. Zhang, J. Ren and X. Qu, *Angew. Chem. Int. Ed.*, 2016, **55**, 6646−6650.

124 T. Yang, A. S. Fruergaard, A. K. Winther, A. N. Zelikin and R. Chandrawati, *Small*, 2020, **16**, 1906744.
125 C. Zhang, L. Chen, Q. Bai, L. Wang, S. Li, N. Sui, D. Yang and Z. Zhu, *ACS Appl. Mater. Interfaces*, 2022, **14**, 27720−27732.
126 J. Liu, W. Zhang, M. Peng, G. Ren, L. Guan, K. Li and Y. Lin, *ACS Appl. Mater. Interfaces*, 2020, **12**, 29631−29640.
127 X. Mu, J. Wang, H. He, Q. Li, B. Yang, J. Wang, H. Liu, Y. Gao, L. Ouyang, S. Sun, Q. Ren, X. Shi, W. Hao, Q. Fei, J. Yang, L. Li, R. Vest, T. Wyss-Coray, J. Luo and X. D. Zhang, *Sci. Adv.*, 2021, **7**, eabk1210.
128 R. P. Mason, M. Casu, N. Butler, C. Breda, S. Campesan, J. Clapp, E. W. Green, D. Dhulkhed, C. P. Kyriacou and F. Giorgini, *Nat. Genet.*, 2013, **45**, 1249−1254.